# A Wavelet Space-Scale-Decomposition Analysis of Structures and Evolution of QSO's Ly$\alpha$ Absorption Lines

Jesus Pando and Li-Zhi Fang

Department of Physics, University of Arizona, Tucson, AZ 85721

**Abstract**

A wavelet space-scale decomposition (SSD) analysis of large scale structures in the universe has been developed. The SSD method of identifying and measuring structures in the spatial distribution of objects has been demonstrated. The position and strength (richness) of the identified clusters can be described by the corresponding coefficient of the wavelet transform. Using this technique, we systematically detected the clustering and its evolution of QSO's Ly$\alpha$ forest lines in real data and simulated samples. We showed that the clusters of Ly$\alpha$ absorbers do exist on scales as large as at least 20 $h^{-1}$ Mpc at significance levels of 2-4 $\sigma$. Independent data sets show about the same strength distribution of the decomposed clusters. The number densities of the clusters on scales of 10 - 20 $h^{-1}$ Mpc are found to evolve in an opposite sense as that of the lines themselves, i.e. they decrease with redshift. We also showed that the number density and the strength distribution of clusters can play an important role in testing or discriminating models, i.e. it can distinguish real data and simulated samples, which cannot be discriminated by traditional ways. We used Daubechies 4 and Mallat wavelets as the bases of the SSD. All above-mentioned conclusions do not depend on either wavelet basis.

**Key words:** Ly$\alpha$ forest - large scale structure - cosmology

## 1. Introduction

It is generally believed that the Ly$\alpha$ absorption line forest in QSO spectra comes from intervening absorbers, or clouds, with neutral hydrogen column densities ranging from about $10^{13}$ to $10^{17}$ cm$^{-2}$ at high redshifts. The spatial distribution of the absorption lines in the forests should, in principle, be able to be used to yield information concerning the formation and evolution of cosmic clustering on much larger scales than do galaxies. Since the Ly$\alpha$ clouds are much more numerous than QSOs, and since Ly$\alpha$ forest samples suffer less from selection effects, one can expect that Ly$\alpha$ forest systems are good tracers of matter distributions on larger scales, and that they might reveal some aspects of cosmic structure formation at redshifts from $z \sim 1$ - 4.

However, the problem of clustering in Ly$\alpha$ forest systems is seriously controversial. Systematic searches for the physical clustering of Ly$\alpha$ absorption lines began in the early 1980's. The first study of the distribution of redshifts in the QSO Ly$\alpha$ forest (Sargent *et al.* 1980) concluded that no structures could be identified. Almost all of the results drawn from two-point correlation function analysis have failed to detect any significant correlation on the scale in velocity space from $\sim$ 300 to 30,000 km s$^{-1}$. The first detection of the correlation of Ly$\alpha$ clouds were made only on size scales of 50-290 km s$^{-1}$ by Webb (1987), see also Rauch et al. (1993). In fact, the absence of power in the two-point correlation function has been claimed as a striking characteristic of the Ly$\alpha$ forest (Weymann 1993).

On the other hand, a series of works based on other methods have detected the deviation of Ly$\alpha$ forests from uniform or random distributions with high confidence. For instance, the distribution of nearest neighbor Ly$\alpha$ line interval is found to be significantly different from a Poisson distribution (Duncan, Ostriker, & Bajtlik 1989; Liu and Jones 1990;). Crotts (1989) directly identified a void with comoving size 40 h$^{-1}$ Mpc (where h is the

Hubble constant in units of 100 km/s Mpc) in the Ly$\alpha$ forest of Q0420-388. Subjecting the same data of Crotts to a method based on Kolmogorov-Smirnoff (K-S) statistic, Fang (1991) showed that Ly$\alpha$ absorbers deviate from a uniform distribution on scales as large as 30-50 $h^{-1}$ Mpc at $\sim 3\sigma$ significant level. Contrary to the results obtained using the two point correlation function, these studies indicate that there should exist large scale structures in Ly$\alpha$ forest.

The difference in the conclusions reached by the different methods is due mainly to the inefficiency of the two-point correlation function in detecting large scale structures. Since to determine the two-point correlation function a good estimate of mean density of the sample is needed, any statistic based on the amplitude of the two-point correlation function of objects is insensitive in detecting structures on size scale $r$ if the uncertainty in the mean density of the sample is comparable to the mean density enhancement given by a structure over the size scale $r$. In a word, two-point correlation function is not infrared (long wavelength) stable. On the other hand, it is impossible to accurately determine the mean density from observed samples because of the lack of information of the object's distributions on scales larger than the sizes of samples considered. The problem is more severe for the study of high redshift objects like QSO absorption systems, because the mean number density of the lines is redshift-dependent. As Liu and Jones (1990) have shown, some information on clustering of Ly$\alpha$ clouds, especially on large scales, is lost in two-point correlation function analysis due to the effects of the finite size of the sample and the uncertainty of mean number density of lines. The methods of nearest neighbor line interval and K-S statistics do not give information of strength and positions of individual structures in the spatial distribution of the Ly$\alpha$ absorbers, as these measures are global.

To overcome this difficulty, a statistic based on the change in the shape, but not on the amplitude, of the two-point correlation function has been proposed (Mo et al. 1992a,

1992b, Einasto & Grasmann 1993, Deng, Xia & Fang 1994). This method succeeded in detecting typical scales in the large-scale structure. It was found that some typical scales in the distribution of QSO Ly$\alpha$ systems are in good agreement with that in the distribution of galaxies and clusters of galaxies (Mo et al. 1992a, b). However, this method, like all others based on the two-point correlation function, can only detect the scales of the clustering, but not the location of the structures. Moreover, the choice of bin size or the smoothing length in the two-point correlation statistics leads to an uncertainty in detecting correlation scales, especially the binning usually uses a top-hat function which contains components of all wavelengths in Fourier space.

In this paper, we propose to investigate this problem by the method of space-scale-decomposition (SSD) based on discrete wavelet transform. We choose this method because it has been found to be a perfect mathematic tool to systematically detect structures on various scales in samples of turbulence and multi-particle physics (Farge 1992, Greiner, Lipa & Carruther 1993). The discrete wavelet SSD possesses a series of mathematical features including space-scale locality, completeness, invertibility, orthogonality. These properties guaranteed that the infrared uncertainty will be avoided. The structures can then be identified and measured *simultaneously* in terms of its scale and position.

The goals of this paper are two-fold. First, we develop the wavelet SSD method of identification and description of structures on various scales in 1-dimension LSS samples. Second, using this technique, we analyze the structures and its evolution in the spatial distribution of Ly$\alpha$ forest lines. A series of features, which have never been detected by traditional methods, are found: 1) the clusters of Ly$\alpha$ absorption clouds do exist on scales as large as, at least, 20 $h^{-1}$ Mpc at 2-4$\sigma$ level; 2) the number density of these clusters show an opposite evolution with that of absorption lines, i.e. the number of the clusters are decreasing with redshifts; 3) the number density, strength distribution and evolution

of these clusters can effectively distinguish real data with some linear simulation samples, which passed all tests before the wavelet SSD analysis. Therefore, wavelet SSD is not only a good mathematical technique, but a necessary tool to revealed new physical problems of LSS.

The paper is arranged as follows. In §2, the method of wavelet SSD analysis is presented. §3 demonstrated the SSD's identification and description of structures in simulation samples of Ly$\alpha$ forests. In §4 we show the results of systematic detection of clusters of QSO's Ly$\alpha$ absorption lines in two real data sets. The evolution of the number density of clusters on various scales, and its comparison with a dynamical models is studied in §5. Finally, conclusion and discussion is in §6.

## 2. Space-scale decomposition of wavelet transform

### *2.1 The need for wavelet space-scale decomposition*

Space-scale decomposition (SSD), or multiresolution analysis, is not new in large scale structure study. Many existing methods for identifying clusters and groups from galaxy surveys can be classified as SSD. These include: a) identification of structure simply by *eyes*, b) percolation, c) friend-to-friend algorithm, d) smoothing by a window function, or filtering technique; e) Fourier transform on finite domain, etc. Strictly speaking, SSD is a technique designed for resolving an arbitrary function simultaneously in terms of its standard variable (say position) and its conjugate counterpart in Fourier space (in this case wavenumber) in an efficient manner. Because of this requirement, no one among the above listed methods is qualified. A complete and consistent SSD should satisfy all the following conditions.

1. Space-scale locality. By definition, the space-scale decomposed components should be localized on both physical and scale (Fourier) space. The basis for the decomposition should be functions which are concentrated on finite domain and vanish outside a domain

of compact support. This requirement excludes the standard Fourier transform, because the information content of a distribution is completely delocalized among all the spectral coefficients. The methods of smoothing by discontinues functions, such as the popular window – the top-hat function, should also be excluded as there are not localized in Fourier space.

2. Completeness. The basis for the decomposition should be complete because the goal of SSD is not only to identify special type of structures, but to decompose samples into objects on all scales, regardless the strength of the clustering. This requirement excludes, at the very least, any method based on identifying structures simply by "eye."

3. Invertibility. Like the Fourier transform, the transform from sample space to SSD coefficient space should be invertible because we need to re-construct the distribution on different scales. This precludes smoothing and passband filtering techniques, which do not give exact reconstruction formulae for synthesizing the sample from the smoothed distributions.

4. Orthogonality. This requirement guarantees no mixing between different space-scale domains. Friends-of-friends, percolation and related methods are ruled out by this requirement. In fact, even continuous wavelet transforms should also be ruled out because continuous wavelets form an overcomplete basis, and their basis functions are not orthogonal. As a consequence, the continuous wavelet transform of a random sample shows some correlations that are obviously not in the sample, but in the wavelet transform coefficients themselves. Therefore, continuous wavelet transforms used in all previous wavelet studies of LSS (Slezak, Bijaoui & Mars 1990; Escalera & Mazure 1992; Escalera, Slezak & Mazure 1992; Martinez, Paredes & Saar 1993) are not appropriate for SSD. On the other hand, the discrete wavelet transform allows an orthogonal projection on a minimal number of independent modes. In this case, all wavelet coefficients are uncorrelated. Therefore,

the difference between continuous and discrete wavelets is essential, unlike the case for the Fourier transform, for which the difference of the continuous and discrete basis is technical.

5. Optimization. The orthogonal basis of wavelet transform are obtained by (space) translation and (scale) dilation of one mother function (Meyer 1992; Daubechies 1992). These translation-dilation procedure allows an optimal compromise in view of the uncertainty principle. Namely, the wavelet transform gives very good spatial resolution on small scales, and very good scale resolution on large scales. The Fourier transform on a finite domain is not optimized because it is based on trigonometric functions exhibiting increasingly many oscillations in a window of constant size. In this case the spatial resolution on small scales and the range on large scales are limited by the size of the window.

Therefore, the discrete wavelet transform SSD should be the best among existing methods of SSD.

*2.2 Basic formulae of wavelet SSD*

Any one-dimensional sample of point distributions, like Ly$\alpha$ absorption lines, in the interval [0-1] with resolution $\Delta x$, can be expressed as a histogram $f(x)$ with $2^{-J}$ bins

$$f(x) = f^{(J)}(x) = \sum_{k=0}^{2^J-1} f_{Jk}\phi^T_{Jk}(x) \tag{1}$$

where $J$ is an integer to be determined by

$$J = \mathrm{mod}(|\ln \Delta x|/\ln 2) + 1, \tag{2}$$

and $f_{Jk}$ is the value of $f(x)$ in bin $k2^{-J} \le x \le (k+1)2^{-J}$. $\phi^T_{Jk}(x)$ in eq.(1) are given by

$$\phi^T_{jk}(x) = \begin{cases} 1 & \text{for } k2^{-j} \le x \le (k+1)\,2^{-j} \\ 0 & \text{otherwise.} \end{cases} \tag{3}$$

where $0 \leq k \leq 2^j - 1$. The superscript $T$ denotes $\phi$ being a top-hat function. Obviously, $\phi^T_{jk}(x)$ can be re-written as

$$\phi^T_{jk}(x) = \phi^T\,(2^j x - k), \tag{4}$$

where $j$, $k$ are integer, $0 \leq k \leq 2^j - 1$, and $\phi^T(x)$ the top-hat mother function

$$\phi^T(x) = \begin{cases} 1 & \text{for } 0 \leq \mathrm{x} \leq 1 \\ 0 & \text{otherwise.} \end{cases} \tag{5}$$

Obviously, $\phi^T_{00} = \phi^T(x)$. Eq.(4) means that functions $\phi^T_{jk}(x)$ are constructed from mother functions (5) by dilating a factor $2^j$, and translating a number $k$.

In the function $\phi^T_{jk}(x)$, the index $j$ denotes the spatial scale and $k$ the position. For a given scale $j$ functions $\phi^T_{jk}(x)$ are orthogonal with respect to the index $k$. Since the resolution in $x$-space is equal to or no finer than $\Delta x$, $f^J(x)$ is the expression of $f(x)$ on finest scale $J$.

In order to find the distribution $f(x)$ on scale $J-1$, we should expand $f(x)$ into $\phi^T_{J-1,k}(x)$. However, this expansion cannot simply be found by eq.(1), because $\phi^T_{J-1,k}(x)$ are not orthogonal to the finer resolution functions $\phi^T_{Jk}(x)$. To solve this problem, we consider a difference function defined by

$$\psi^T(x) = \begin{cases} 1 & \text{for } 0 \leq x \leq 1/2 \\ -1 & \text{for } 1/2 \leq x \leq 1 \\ 0 & \text{otherwise.} \end{cases} \tag{6}$$

Similarly, one can construct $\psi^T_{jk}(x)$ by dilating and translating eq.(6) as

$$\psi^T_{jk} = \psi^T(2^j x - k) = \begin{cases} 1 & \text{for } k2^{-j} \leq x \leq (k+1/2)\ 2^{-j} \\ -1 & \text{for } (k+1/2)2^{-j} \leq x \leq (k+1)\ 2^{-j} \\ 0 & \text{otherwise.} \end{cases} \tag{7}$$

Functions $\psi^T_{jk}(x)$ are orthogonal with respect to *both* indexes $j$ and $k$. For a given $j$, $\psi^T_{jk}(x)$ are also orthogonal to functions $\phi^T_{jk}(x)$. $\psi^T_{jk}(x)$ and $\phi^T_{jk}(x)$ are usually called the wavelet and scaling functions, respectively.

From eqs.(4) and (7), we have

$$\begin{aligned} \phi^T_{j,2k}(x) &= \tfrac{1}{2}(\phi^T_{j-1,k}(x) + \psi^T_{j-1,k}(x)), \\ \phi^T_{j,2k+1}(x) &= \tfrac{1}{2}(\phi^T_{j-1,k}(x) - \psi^T_{j-1,k}(x)), \end{aligned} \tag{8}$$

where $0 \leq k \leq 2^{j-1} - 1$. Eq.(8) shows that all scaling functions, $\phi^T_{jk}(x)$, can be expressed by wavelets *and* scaling functions on scale $j-1$. For this property, $\psi(x)$ is called father functions.

From eqs.(1) and (8), it is easy to show that

$$f^J(x) = \sum_{k=0}^{2^{J-1}-1} f_{J-1,k}\phi^T_{J-1,k}(x) + \sum_{k=0}^{2^{J-1}-1} \tilde{f}_{J-1,k}\psi^T_{J-1,k}(x) \tag{9}$$

where the mother function coefficient (MFC), $f_{J-1,k}$, and father function coefficient (FFC), $\tilde{f}_{J-1,k}$ are given by

$$\begin{aligned} f_{J-1,k} &= \tfrac{1}{2}(f_{J,2k} + f_{J,2k+1}), \\ \tilde{f}_{J-1,k} &= \tfrac{1}{2}(f_{J,2k} - f_{J,2k+1}). \end{aligned} \tag{10}$$

In eq.(9), The term containing the mother functions gives the distribution $f(x)$ on scale $J-1$, and the term containing the father functions contains the information of the difference between scales of $J$ and $J-1$. Since $\psi^T_{J-1,k}(x)$ are orthogonal to $\phi^T_{J-1,k}(x)$, the mother function term is not mixed with any components on scales $J$. Therefore, one can safely describe the distribution $f(x)$ on scale $J-1$ by

$$f^{J-1}(x) = \sum_{k=0}^{2^{J-1}-1} f_{J-1,k}\phi^T_{J-1,k}(x) \tag{11}$$

One can repeat this procedure to find the distribution on scale $J-2$ from scale $J-1$. Thus, the distribution $f(x)$ can be decomposed into $f^j(x)$ with $0 \leq j \leq J$. For scale $j$, the distribution $f^j(x)$ is totally determined by the MFC $f_{j,k}$.

For largest scale $j = 0$, we have $f^0(x) = f_0^0 \phi_{00}^T(x)$, and

$$f^J(x) = f_0^0 \phi_{00}^T(x) + \sum_{j=0}^{J-1} \sum_{k=0}^{2^j-1} \tilde{f}_{jk} \psi_{jk}^T(x) \tag{12}$$

Obviously, the MFC $f_0^0$ now is simply the mean density of points on interval $[0, 1]$. Since functions $\psi_{jk}^T(x)$ are orthogonal with respect to $j$ and $k$, the FFCs can be calculated by

$$\tilde{f}_{jk} = 2^j \int f(x) \psi_{jk}^T dx \tag{13}$$

MFC at various scales can be found from $f_0^0$ and FFCs $\tilde{f}_{jk}$.

All the above discussions are based on the top-hat wavelet. As we mentioned in the last section, the to-hat function (5) and difference function (6) are discontinues, and so are not good for SSD. Nevertheless, many formulae developed above still hold for all wavelet transforms. For instance, eq.(13) should be fundamental for any mother functions. In the mid-80's to early 90's there was a great deal of work in trying to find a continuous basis that was well localized in Fourier space (Daubechies et al. 1986, Daubechies 1990, Mallat 1989, Mallat & Zhong 1990, Meyer 1986). Specifically, Daubechies (1988) constructed several families of wavelets and scaling functions which are orthogonal, have compact support and are continuous. The wavelet function $\psi_{jk}(x)$ and the scaling function $\phi_{jk}(x)$ are defined as

$$\phi(x) = \sum_m c_m \, \phi(2x - m) \tag{14}$$

$$\psi(x) = \sum_m (-1)^m c_{1-m} \, \phi(2x - m) \tag{15}$$

where the coefficients $c_m$ must satisfy proper conditions (Daubechies 1988). If the nonzero coefficients $c_m$ are taken to be $c_0 = c_1 = 1$, we have the top-hat scaling and wavelet (5) and (6). The simplest wavelet function $\psi(x)$ which is dually localized in both $x$-space and Fourier-space is given by filter $c_0 = (1 + \sqrt{3})/4$, $c_1 = (3 + \sqrt{3})$, $c_2 = (3 - \sqrt{3})/4$ and $c_3 = (1 - \sqrt{3}/4)$. It is often called wavelet D4. In our SSD analysis, the decomposition

was mainly done by the D4, but we also check the reliability of the SSD results by using wavelets of D12, D20 and Mallet (1989).

## 3. A Demonstration of structure identification by wavelet SSD

In order to demonstrate the method of wavelet SSD, we did a SSD analysis of simulation samples of Ly$\alpha$ forests covering redshift range from 1.7 to 4.1 (Bi 1993; Bi, Ge & Fang 1994, hereafter BGF). The density field in this simulation are generated as Gaussian perturbations with linear power spectrum given by cosmological models of the standard cold dark matter (SCDM), the cold plus hot dark matter (CHDM), and the low-density flat cold dark matter (LCDM). Within a reasonable range of $J_\nu$, the UV background radiation at high redshift, the sample of LCDM model is found to be in good agreement with observational features including 1) the number density of Ly$\alpha$ lines and its dependencies on redshift and equivalent width; 2) the distribution of equivalent widths and its redshift dependence; 3) two-point correlation function; and 4) the Gunn-Peterson effect.

Since the perturbation spectrum used for the simulation is not white noise, the distribution of Ly$\alpha$ absorption lines in BGF samples should contain large scale structures. However, the two point correlation function of lines in redshift (or velocity) space detected nothing from these samples. A typical result of the two-point correlation function of a BGF sample best fitting observations is plotted in Figure 1. As is the case with observations, the simulated samples showed no power of line-line correlations on scales of about 100 km s$^{-1}$ to 2000 km s$^{-1}$. These results clearly show that the two-point correlation function sometimes is ineffective in detecting structures on large scales.

We then subjected the best fitting sample of the BGF data to a SSD analysis by the D4 wavelet. First, we formed one dimensional distribution $f(x)$ of Ly$\alpha$ lines by writing each sample in BGF into histogram with bins of $\triangle z = 0.0025$, which was about the resolution with which the data was produced. We then generated 100 random samples for each

simulation sample. To consider the influence of evolution of the number of lines, the total number of lines and the number of lines within a given red-shift interval (say, $\triangle z = 0.4$) of the random samples are chosen to match the parent distribution. We calculated the FFC $\tilde{f}_{jk}$ and MFC $f_{jk}$ for both the BGF sample and the random data. In fact, these amplitudes can easily be obtained via linear transformations from data space into wavelet space by a wavelet transformation matrix (Press et al. 1991).

Using MFCs, one can reconstruct the density field $f^j(x)$ on the scale being considered. Figure 2 shows a result of reconstructing a BGF sample on scales $j = J-1, J-2$ and $J-3$, where $J$ the finest (resolution) scale, and $J-1,\ J-2,\ J-3$ correspond to scales (in comoving space) of about 5, 10 and 20 $\mathrm{h}^{-1}$ Mpc, respectively. In the reconstructed field the density is sometimes negative (see Figure 2) because the mother function of D4 are somewhere is negative. For structure identification we don't really need a reconstructed field, but only the MFCs. This shows that the wavelet reconstruction is not simply a smoothing technique.

Since the MFCs, $f_{jk}$, describes the strength of density field at position $k$ and on scale $j$, we can identify the clusters by calculating the MFC's difference between simulated sample and random data. Figure 3 shows a part of the result of the difference of MFCs between a BGF sample and random distribution. The error bars are $1\sigma$ around the average of the MFC's differences given by 100 random sample. From Figure 3, one can easily pick out the peaks, each of which is described by position ($k$) and height of the coefficient difference. The clusters of Ly$\alpha$ absorption lines are then identified as these peaks. The scale of these clusters is given by $j$, the location of clusters is shown by the position of peaks, and the strength or richness of the clusters can be measured by the height/$\sigma$.

Figure 4 shows the total number $N(> R)$ of clusters with strength larger than $2\sigma$ on scales $J-1,\ J-2,$ and, $J-3$. To test this identification we analyzed 20 BGF simulation

samples with the same cosmological parameters. The error bar in Figures 4 is given by the average among the 20 simulated samples. One can conclude that the structures in the line distribution have been systematically detected on scales $j-1,\ j-2,$ and $j-3$. The identified structures are at significance levels of 2-4 $\sigma$. It is clear that the wavelet SSD has accomplished what the two point correlation function could not. The function $N(>R)$ describes the strength (or richness) distribution of the identified clusters.

## 4. Clusters of Ly$\alpha$ absorbers

Having had the wavelet SSD successfully analyze the simulated BGF data, we now turn to identifying the clusters of Ly$\alpha$ absorbers from real data. We should first point out that the word "clusters" used here does not imply that they are virialized and gravity-confined systems. SSD identified clusters are not defined by dynamical features like clusters of galaxies, but only by density distributions. This is not a weakness, but probably an advantage of wavelet SSD.

Recent measurements have found that the size of the Ly$\alpha$ clouds at high redshift is unexpectedly as large as 100 - 200 $h^{-1}$ Kpc, and their velocity dispersion is unexpectedly as low as $\sim 100$ km $s^{-1}$ (Bechtold et al. 1994, Dinshaw et al. 1995). These results cannot be matched with the pictures of pressure equilibrium and virialization. For instance, if the Ly$\alpha$ clouds with such large size are well gravitationally confined, the Press-Schechter theory shows that their column density should be equal to or larger than $10^{17}$ $cm^{-2}$ (Mo, Miralda-Escudé & Rees 1993). Clouds with large size and low column densities are not completely gravity-confined. Therefore, the Ly$\alpha$ clouds are probably neither virialized nor completely gravity-confined, but given by pre-collapsed areas in the density field.

Therefore, identification of dynamically pre-collapsed clusters (or dense areas) is important, especially for understanding structure formation at high redshifts. The wavelet SSD would be able to uniformly identify clusters with various strength, i.e. at various

evolutionary stage.

*4.1 Samples and identification*

We look at two data sets of the Ly$\alpha$ forests. The first was compiled by Lu, Wolfe and Turnshek (1991, hereafter LWT). It contains totally $\sim$ 950 line from the spectra of 38 QSO that exhibit neither broad absorption lines nor metal line systems. The second is from Bechtold (1994), which contains a total $\sim$ 2800 lines from 78 QSO's spectra, in which 34 high redshift QSOs were observed at moderate resolution. In our statistics, the effect of proximity to $z_{em}$ has been considered. All lines with $z \geq z_{em} - 0.15$ were deleted from our samples. As with other data sets, no power of two point correlation function was detected from these two compiled samples on large scales.

We treated the data as discussed in the previous section. We assumed $q_0 = 1/2$, so the distance of an absorber at redshift $z$ is given by $d = 2(c/H_o)[1 - (1+z)^{-1/2}]$. The samples range from a comoving distance of about 2,500 $h^{-1}$Mpc to 3,300 $h^{-1}$Mpc. Each QSO's spectrum was analyzed individually, i.e. for each QSO 100 random trials matching the line numbers in each redshift range of the parent sample were generated. Similar to Figure 3, Figure 5 shows a part of the MFC difference for the forest of QSO-0237. The errors are also the $1\sigma$ found from the average over the 100 subtractions between MFCs of real data and random samples. Figure 5 is typical for all QSO's analyzed. It is interesting to note from Figure 5 that the $j = J - 1$ clusters shown around 2465-2480 $\mathrm{h}^{-1}$ Mpc also appear as $j = J - 2$ and $j = J - 3$ clusters at the same place. That is this structure appears at all three resolution scales, $j = J - 3$, $j = J - 2$ and $j = J - 1$. Differently, the structure appearing at 2505-2520 Mpc only appears on the scales $j = J - 1$ and $j = J - 2$, but not on larger scales.

*4.2 Number and strength of clusters*

In Figures 6, 7 and 8 we show the total number $N(> R)$ of clusters detected with the strength $R > 2\sigma$ for both the LWT and Bechtold data. It is interesting to note from Figures 6 and 7 that the two independent data sets show statistically the same strength distributions of the clusters consisting of $W > 0.32\mathring{A}$ lines. However, comparing these results with the BGF's clusters (Figure 4), the drop of $N(> R)$ of real data is obviously slower than for the simulated BGF data. That is, the abundance of rich clusters in real data is higher than simulated samples. From Figures 4, 6 and 7, one can find that among all $j = J - 1$ clusters of $> 2\sigma$, the abundances of $R > 3.5\sigma$ clusters is 7% for BGF sample, 23% for LWT data, and 28% for Bechtold data. The difference of $R > 4\sigma$ cluster abundance between real and simulated sample is more remarkable. Almost no $R > 4.5\sigma$ clusters are detected in BGF samples, while they do exist in the real data. This indicates that in linear simulations the rich clusters are underestimated.

As very well known, the spatial clustering of Ly$\alpha$ absorbers can be smeared out by peculiar motion of the absorbers. The influence of peculiar velocity is difficult to estimated because the velocity distributions of absorbers is not clearly understood. However, on the scales equal to or larger than about 5 $h^{-1}$ Mpc, the influence of peculiar motions should be negligible. Therefore, the identified clusters on scales $j = J-1$, $j = J-2$ and $j = J-3$ should be more reliable than the original lines as a tracers of matter distribution on large scales.

In order to test the stability of the number of the identified clusters with respect to the choice of wavelets, we repeated the SSD analysis by using the Mallet wavelet basis, which is more soft than the D4. Figure 9 shows the number of the identified ($> 2\sigma$) clusters from the LWT data. Comparing Figure 6 and 9, one finds that the total number of the $R > 2\sigma$ clusters on $j = J - 1$ and $j = J - 2$ is almost identical for both wavelets. The total number of structures at $j = J - 3$ shows a slight difference, but is of no statistical

significance.

## 5. Redshift-dependence of clusters

Using the samples of clusters identified from the wavelet SSD, one can study all aspects of interest for large scale structure formation: the number density, correlation function, their redshift-dependence (evolution), scale- and strength-dependence etc. That is, SSD opens new fields to compare observations with models. We can conduct the testing and discriminating of models by a scale-to-scale confrontation. In this paper, as an example, we only show a scale-to-scale study of the number density and its redshift-dependence of the clusters of Ly$\alpha$ absorbers.

### *5.1 Evolution of number density*

It is generally believed that the number of Ly$\alpha$ forest lines increases with redshift. The redshift-dependence of the number density of lines with rest equivalent width $W$ greater than a threshold $W_{th}$ can be described as

$$\frac{dN}{dz} = \left(\frac{dN}{dz}\right)_0 (1+z)^{\gamma} \ , \tag{16}$$

where $(dN/dz)_0$ is the number density extrapolated to zero redshift, and $\gamma$ the index of evolution. If the absorbers distribution is comoving in a flat universe, the number density should be $(dN/dz) \propto (1+z)^2/[\Omega(1+z)^3+\lambda]^{1/2}$, where $\lambda$ is the cosmological constant. The deviation of $dN/dz$ from the comoving curve implies an evolution of the population of Ly$\alpha$ clouds. In the case of $\lambda = 0$, $\gamma > 0.5$ implies that the number of Ly$\alpha$ clouds increases with redshift, and $\gamma < 0.5$ decreases with redshift. The index $\gamma$ is found to depend on $W_{th}$: in general the larger $W_{th}$, the higher $\gamma$.

The simple power law, eq.(16), cannot cover the entire redshift range being examined. The parameters $(dN/dz)_0$ and $\gamma$ are found to be different at different redshift ranges.

Although the $dN/dz$ given by different groups showed a common evolutionary trend, there are differences in amplitude $(dN/dz)_0$ by a factor of about 30%. LWT (1991) showed that $(dN/dz)_0 \simeq 3$ and $\gamma = 2.75 \pm 0.29$ for lines with $W \geq W_{th} = 0.36\mathring{A}$ and in the redshift range $1.6 < z < 4$. Bechtold (1994) found $\gamma = 1.89 \pm 0.28$ for $W_{th} = 0.32\mathring{A}$ and $\gamma = 1.32 \pm 0.24$ for $W_{th} = 0.16\mathring{A}$. This smaller value seems to be consistent with the low-redshift results from the Hubble Space Telescope (Morris et al. 1991; Bahcall et al. 1991.) It would better to directly compare the curves of $dN/dz - z$, not the parameters $(dN/dz)_0$ and $\gamma$.

We analyzed the evolution of the number density of clusters on scales $j = J - 1$, $j = J - 2$ and $j = J - 3$. The results are plotted in Figure 10, in which 10a is for LWT and 10b for Bechtold data, both the width is taken to be $> 0.32\mathring{A}$. The $dN/dz$ vs $z$ curves of Ly$\alpha$ lines are the same as the LWT's and Bechtold's original results. Namely, both show that the number density of Ly$\alpha$ lines increases with redshift. However, the number densities of $j = J - 1, J - 2, J - 3$ clusters show an opposite evolution, i.e. they are decreasing with redshifts. This result indicates that, along with the possible decline of Ly$\alpha$ lines, the large scale structures traced by Ly$\alpha$ lines were growing during the era $4 > z > 2$. Obviously, this evolutionary scenario would not be able to be revealed without a powerful SSD measurement.

Because we lack sufficient data to provide an accurate analysis of $dN/dz$ of clusters at high redshift, we are reluctant as yet to quantify the index $\gamma$ for the clusters on different scales. Nevertheless, these opposite evolutions should be statistically significant because the two independent data sets (LWT and Bechtold) showed the same amplitude of $dN/dz$, and the same trend of the evolution over the entire redshift range $2 < z < 4$.

*5.2 Testing model by scale-decomposition*

Let us go back to the simulation samples of BGF. We did the same analysis as in the

previous section for the best BGF samples. The result is shown in Figure 11, in which 11A is from BGF sample and 11B from Bechtold data with the same width threshold as BGF, $W > 0.16\mathring{A}$. First, Figure 11 shows that the $dN/dz$ vs $z$ curve of Ly$\alpha$ lines themself of BGF sample is in good agreement with observation. This is one reason we say that this BGF sample is the best. The evolution of the number densities of $j = J-1,\ J-2,\ J-3$ clusters also show the same trend as real data: $dN/dz$ is decreasing with redshift.

However, the number densities given by simulated sample are remarkably different from the real data. The values of $dN/dz$ of $J-1,\ J-2,\ J-3$ clusters for BGF are less than the observational results by a factor of 5-10. Considering both LWT and Bechtold have about the same number density, one cannot explain the difference between BGF and Bechtold as the uncertainty of the current observation. This result once again suggests that the linear simulation underestimated the clustering on large scales. In a word, the number densities of $j = J-1, J-2, J-3$ clusters are effective tools to test models which have passed all tests before the SSD analysis.

## 6. Conclusion

The clustering and evolution of Ly$\alpha$ absorption lines have been systematically detected by wavelet SSD. It has been shown that the clusters of Ly$\alpha$ absorbers do exist on scales as large as at least 20 $h^{-1}$ Mpc at significance level of 2-4 $\sigma$. We found that the evolution of the number densities of the clusters is opposite from the lines themself, i.e. decreasing with redshift. This is probably the first time any one has seen this phenomenon. We also showed that the number density of the clusters, and the strength distribution of the clusters can effectively distinguish real data with some models, which can not be distinguished from observational features without a wavelet SSD description.

Therefore, the wavelet SSD is an efficient, fast and reliable way of detecting structure where other traditional methods have failed. It provides a vehicle for discovering physics

at the dimension of scales. It open the window to study the scale-dependence of various features of clustering. For instance, comparing Figure 10B and 11B, one find that the number densities of $W > 0.16\mathring{A}$ clusters are higher than that of $W > 0.32\mathring{A}$ clusters, this scale-dependence implies that the formation of structure in the universe had undergone a biased clustering with respect to the rest frame equivalent widths of absorbers.

It is not accidental that the wavelet SSD analysis shows its unique role of measuring LSS, because the clustering in the universe is probably multi-scaled. According to the standard picture of the structure formation, the initial perturbations are scale-free. The successively non-linear evolution destroyed the perfect scaling, and the density field was no longer described as a Gaussian superposition of plane waves. Therefore, in terms of localized physical and Fourier spaces, the clustering in the universe would be multiscaled, i.e. the LSS is a superposition of coherent structures with various scales. It has been known that in order to fit with galaxies distribution the spectrum of perturbations in the present universe should contain a set of parameters (e.g. Bardeen et al. 1986), each of which should, in principle, correspond to a scale in the clustering.

Observations also showed the multi-scales. In Ly$\alpha$ forests, at least three scales have been mentioned: 1. 40 $h^{-1}$ Mpc of a void Crotts (1989); 2. 30-50 $h^{-1}$ Mpc from K-S statistic (Fang 1991); 3. 80, and even 120 $h^{-1}$ Mpc from typical scale analysis (Mo, et al. 1992a, b). In the same redshift range, QSO's clustering have also been shown to be multi-scaled. Two correlation scales of $r_0 \sim 6$ $h^{-1}$Mpc (Boyle & Mo 1992), and 13 $h^{-1}$Mpc (Bahcall & Chokshi 1991) were found from the two-point correlation function, and clustering scales of $r \leq 30$ $h^{-1}$Mpc and $\sim 100$ $h^{-1}$Mpc have also been detected by the statistics of average two-point correlation function (Mo & Fang, 1993) and typical scale analysis (Mo, et al. 1992a,b; Einasto & Grasmann 1993, Deng, Xia & Fang 1994), respectively. Some differences among these scales may come from the methods used in

the analysis, but it may be difficult to explain all these results by one scale in clustering.

One can concludes that scale-decomposition is not only mathematically convenient, but also physically necessary. We believe that the wavelet SSD of LSS is a vast new area for exploration. For instance, one can, at least, address the following topics, which would not be able to be reached without a qualified SSD: 1.) The scale-dependence of correlations; 2.) non-Gaussianity and the strength distribution of scale-decomposed clusters; 3.) scale-scale interaction, i.e. the interaction between structures on different scales. We will present the results concerning these questions in succeeding papers.

Both authors wish to thank Drs. Bi, Carruthers, Lipa, and Mo for insightful conversations.

## References


**??**ahcall, J.N., Jannuzi, B.T., Schneider, D.P., Hartig, G.F., Bohlin, R., & Junkkarinen, V. 1991, ApJ, 377, L5

**??**ahcall, N.A. & Chokshi, A. 1991, ApJ, 380, L9

**??**ardeen, J., Bond, J.R., Kaiser, N. & Szalay, A.S. 1986, ApJ, 304, 15

**??**echtold, J. 1994, ApJSS, 91, 1.

**??**echtold, J., Crotts, P.S., Duncan, R.C. & Fang Y. 1994, ApJ, 437, L83

**??**i, H.G. 1993, ApJ, 405, 479

**??**i, H.G., Ge, J., Fang, L.Z. 1994, BAAS, 26, 1331

**??**oyle, B.J. & Mo, H.J. 1992, MNRAS, 260, 952

**??**hu,Y.Q., Fang, L.Z. 1987 in *Observational Cosmology*, eds. A. Hewitt, G. Burbidge, L.Z. Fang, Reidel, Dordrecht, P. 627

**??**rotts, A.P.S. 1989, ApJ, 336, 550

**??**aubechies,I., Grossmann,A., Meyer, Y., 1986 J. Math. Phys. 27, 1271

**??**aubechies, I. 1988, Comm. on Pure and Applied Mathematics, 41, 909

**??**aubechies, I. 1990, IEEE Trans. Inf. Theory, 36, 961

**??**eng, Z.G., Xia, X.Y. & Fang, L.Z. 1994, ApJ, 431, 506

**??**inshaw, N., Foltz, C.B., Impey, C.D., Weymann, R. & Morris, S.L. 1995, Nature, in press

**??**uncan, R.C., Ostriker, J.P. & Bajtlik, S. 1989, ApJ, 345, 39

**??**inasto, J. & Grasmann, M. 1993, ApJ, 407, 443

**??**scalera, E., & Mazure, A. 1992, ApJ, 388, 23

**??**scalera, E., Slezak, E. & Mazure, A. 1992, A&A, 264, 379

**??**ang, L.Z. 1991, A&A, 244, 1

**??**arge, M. 1992, Ann. Rev. Fluid Mach., 24, 395

??reiner, M., Lipa, P., & Carruthers, P. 1993, HEPHY-PUB 587/93

??u, L., Wolfe, A.M., & Turnshek, D.A. 1991, ApJ, 367, 19

??iu X.D., Jones B.J.T. 1990, MNRAS, 242, 678

??allat, S. 1989, Trans. Am. Math. Soc., 315, 69

??allat, S., Zhong, S. 1991, *Wavelets and Their Applications*, Boston, Jones & Bartlett.

??artinez, V.J., Paredes, s. & Saar, E. 1993, MNRAS, 260, 365

??eyer, Y. 1987, *Wavelets, Time-Frequency Methods and Phase Space*, 21

??o, H.J. & Fang, L.Z. 1993, ApJ, 410, 493

??o, H.J., Deng, Z.G., Xia, X.Y., Schiller, P., & Börner, G. 1992a, A&A, 257, 1

??o, H.J., Xia, X.Y., Deng, Z.G., Börner, G. & Fang, L.Z. 1992b, A&A, 256, L23

??orris,S.L.,Weymann, R.J., Savage, B.D., & Gilliland, R.L., 1991, ApJ, 377, L21.

??ress, W.H., Flannery, B.P., Teukolsky, S.A. & Vetterling, W.T. 1992, *Numerical Recipes*, New York; Cambridge University Press

??argent, W.L., Young, P.J., Boksenberg, A., & Tytler, D. 1980, ApJS, 42, 41

??lezak, E., Bijaoui, A. & Mars, G. 1990, A&A, 227, 301

??auch, M., Carswell, R.F., Chaffee, F.H., Foltz, C.B., Webb, J.K., Weymann, R.J., Bechtold, J. & Green, R. F. 1992, ApJ, 390, 387

??ebb, J.K. 1987, in *Observational Cosmology* e. A. Hewitt., G. Burbidge, & L.Z. Fang.

??eymann, R.J. 1992, in *The Environment and Evolution of Galaxies*, ed. Shull, J.M. & Thronson, H.A. Jr. 214 (KLumer Academic Publisher).

??oung,P.J., Sargent, W.L.W. & Boksenberg, A. 1982a, ApJ, 252, 10

??oung,P.J., Sargent, W.L.W. & Boksenberg, A. 1982b, ApJS, 48, 455

**Figure captions**

**Figure 1** A typical two-point correlation function of Ly$\alpha$ forest lines in velocity space. The sample is taken to be a simulation of BGF for model of LCDM with $J_{-21} = 3.0$. The line width is taken to be $W_{thr} \geq 0.16$ Å. The error bars represent 1 $\sigma$.

**Figure 2** Wavelet reconstruction of density fields. A. the original (or scale $J$) line distribution of a BGF sample with $W > 0.16\mathring{A}$. B. C. and D. the reconstructed fields for scale $J-1$, $J-2$ and $J-3$, respectively.

**Figure 3** The difference of mother function coefficients between a BGF and random samples at each position $k$. A. B. and C. Correspond to scales of $J-$, $J-2$ and $J-3$, respectively. The error bars represent one $\sigma$ around the average of the coefficient differences given by 100 random sample.

**Figure 4** The average number $N(> R)$ of clusters identified from BGF samples, where $R$ is the richness of the clusters in unit of $\sigma$. A. B. and C. are for scales $J-1$, $J-2$ and $J-3$, respectively. The error comes from average among 20 BGF samples.

**Figure 5** The same as Figure 3 but for QSO-0237 forest with line width $W > 0.16\mathring{A}$. A. B. and C. are for scales $J-1$, $J-2$ and $J-3$.

**Figure 6** Integral number $N(> R)$ of clusters identified from the LWT data (1991), where $R$ is the richness of the clusters. A. B. and C. are for scales $J-1$, $J-2$ and $J-3$, respectively.

**Figure 7** Integral number $N(> R)$ of clusters identified from a Bechtold data (1994) with $W > 0.32\mathring{A}$, where $R$ is the richness of the clusters. A. B. and C. are for scales $J-1$, $J-2$ and $J-3$, respectively.

**Figure 8** Integral number $N(> R)$ of clusters identified from a Bechtold data (1994) with $W > 0.16\mathring{A}$, where $R$ is the richness of the clusters. A. B. and C. are for scales $J-1$, $J-2$ and $J-3$, respectively.

**Figure 9** The same as Figure 6 but using the Mallat wavelet as the basis functions of SSD. Note that numbers $N(> R)$ are very similar to D4 wavelet, although shape of histogram is slightly different.

**Figure 10** dN/dz vs (1+z). A. LWT data of $W > 0.36\mathring{A}$, B. Bechtold data of $W > 0.32\mathring{A}$. The top curves are given by original Ly$\alpha$ lines. The lower curves are given by clusters on scales $J-1$, $J-2$ and $J-3$.

**Figure 11** dN/dz vs (1+z). A. a BGF sample of $W > 0.16\mathring{A}$, B. Bechtold data of $W > 0.16\mathring{A}$. The top curves are given by original Ly$\alpha$ lines. The lower curves are given by clusters on scales $J-1$, $J-2$ and $J-3$. The amplitudes of the BGF curves of $J-1$, $J-2$ and $J-3$ are much lower than the corresponding amplitudes of Bechtold data.

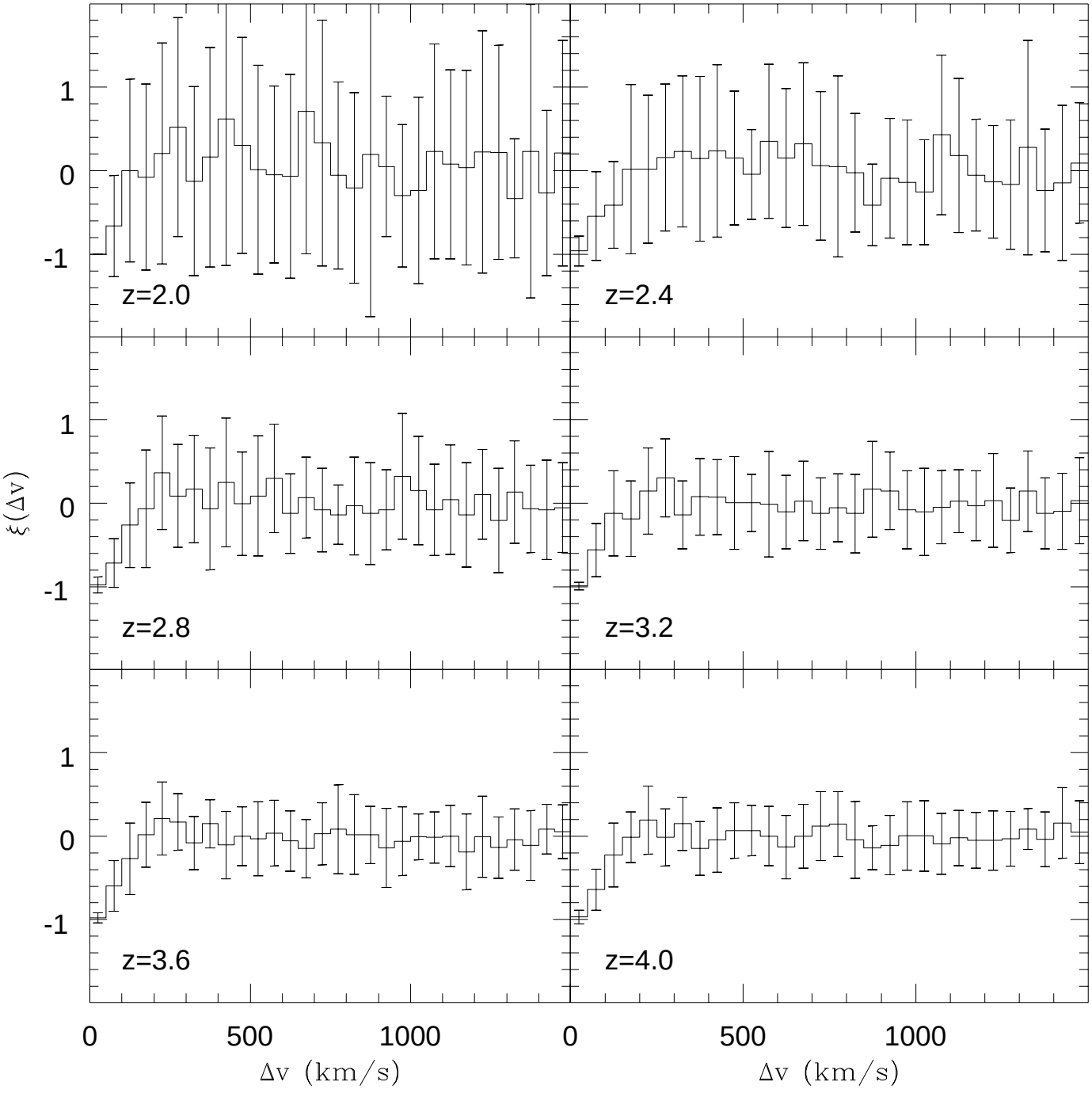


Fig. 1

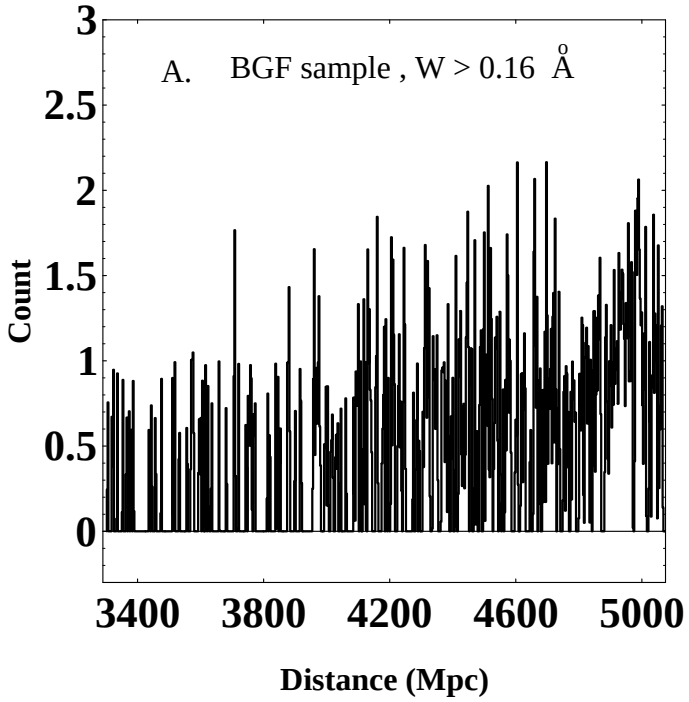
A. BGF sample , W > 0.16 Å
Count
Distance (Mpc)
3
2.5
2
1.5
1
0.5
0
3400
3800
4200
4600
5000

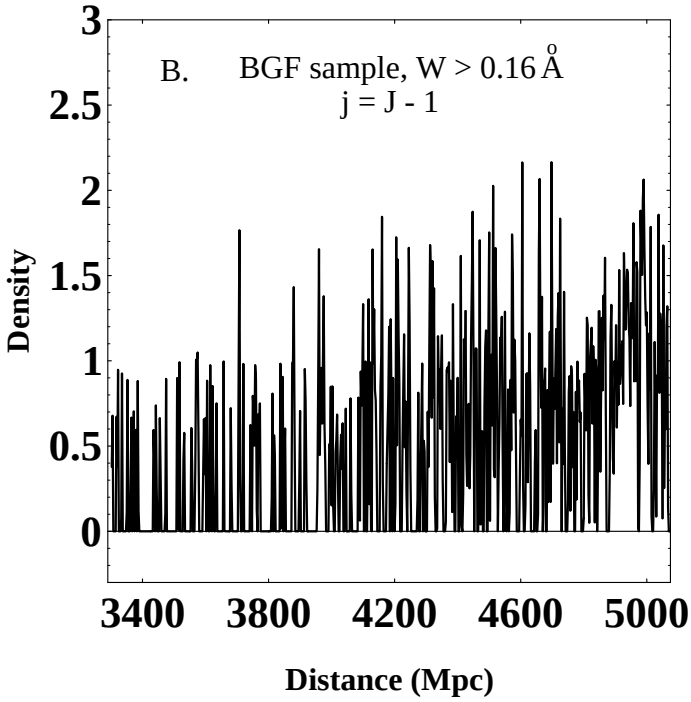
B. BGF sample, W > 0.16 Å
j = J - 1
Density
Distance (Mpc)
3
2.5
2
1.5
1
0.5
0
3400
3800
4200
4600
5000

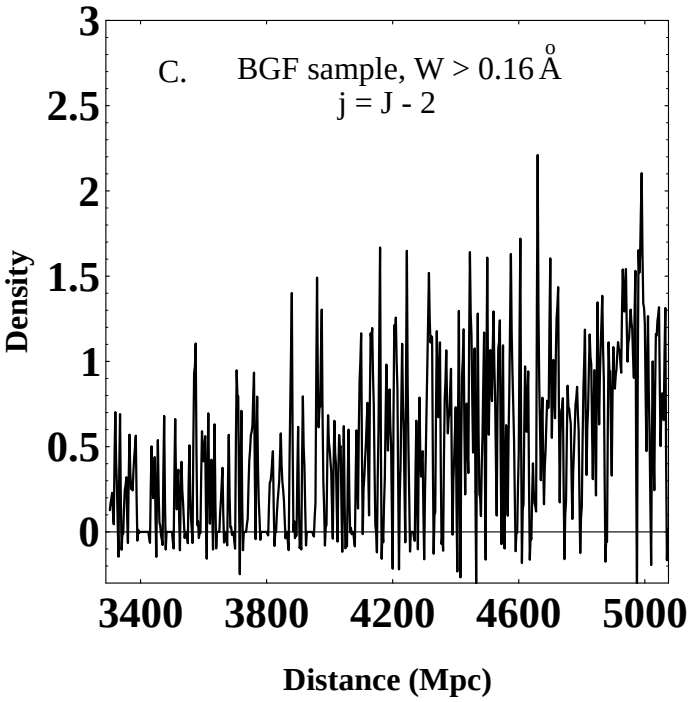
C. BGF sample, W > 0.16 Å
j = J - 2
Density
Distance (Mpc)
3
2.5
2
1.5
1
0.5
0
3400
3800
4200
4600
5000

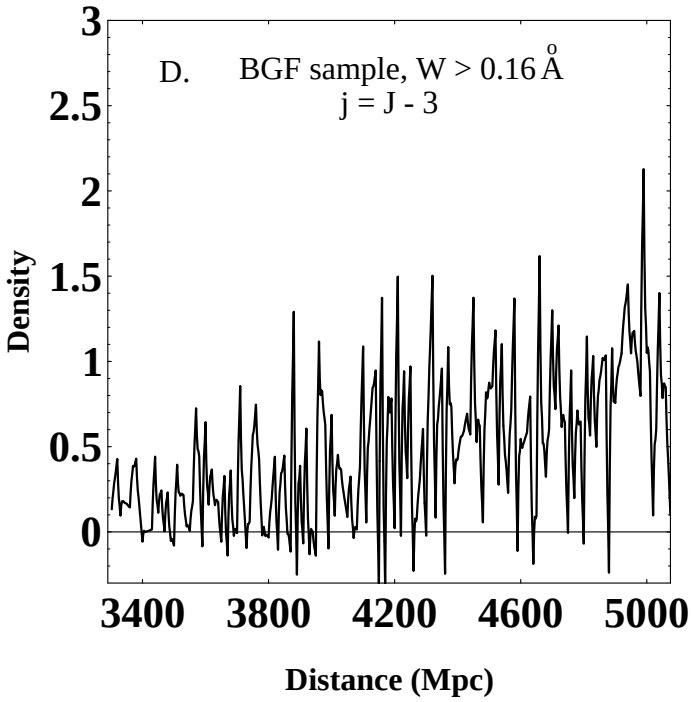
D. BGF sample, W > 0.16 Å
j = J - 3
Density
Distance (Mpc)
3
2.5
2
1.5
1
0.5
0
3400
3800
4200
4600
5000

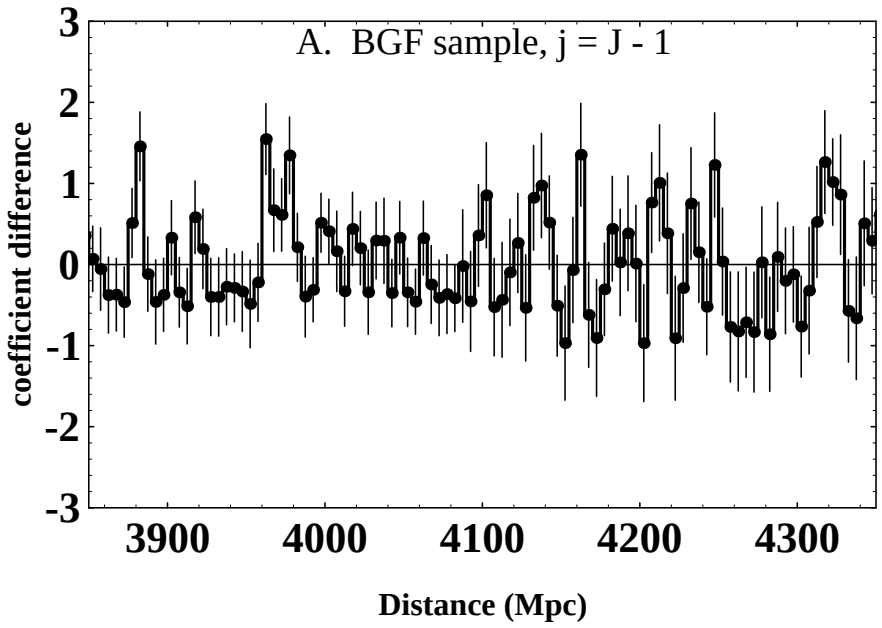
A. BGF sample, j = J - 1
coefficient difference
3
2
1
0
-1
-2
-3
3900
4000
4100
4200
4300
Distance (Mpc)

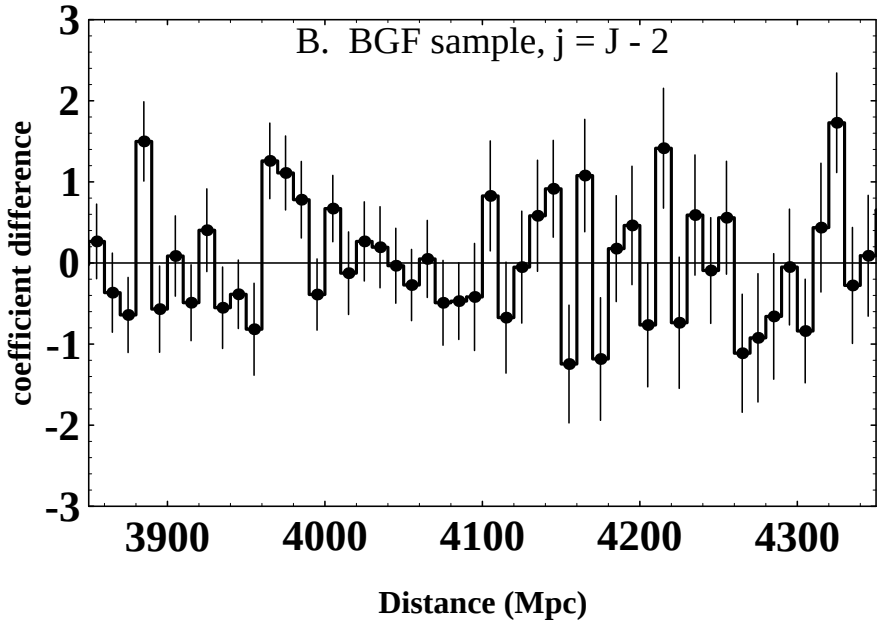
B. BGF sample, j = J - 2
coefficient difference
3
2
1
0
-1
-2
-3
3900
4000
4100
4200
4300
Distance (Mpc)

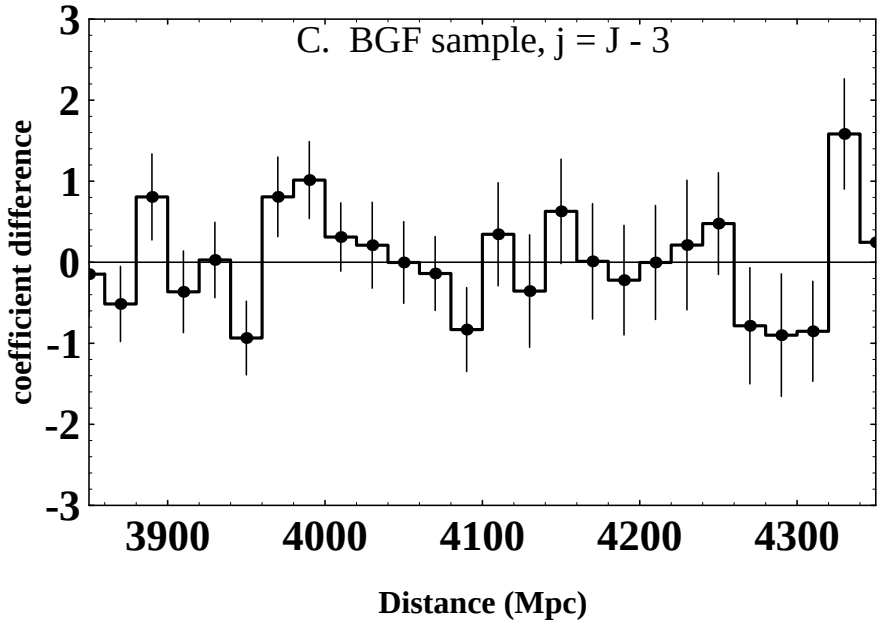
C. BGF sample, j = J - 3
coefficient difference
3
2
1
0
-1
-2
-3
3900
4000
4100
4200
4300
Distance (Mpc)

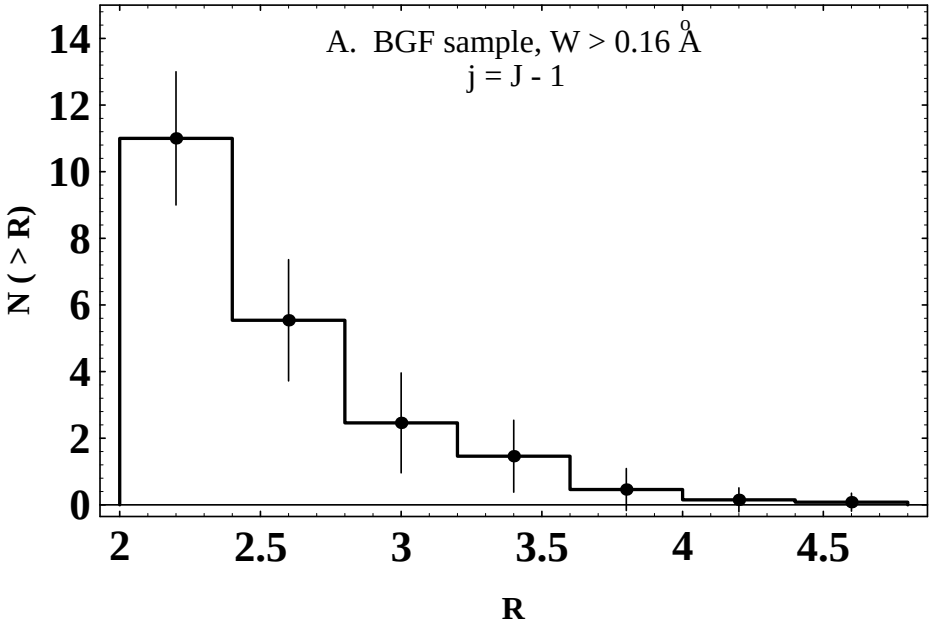
A. BGF sample, W > 0.16 Å
j = J - 1
N ( > R)
R
0
2
4
6
8
10
12
14
2
2.5
3
3.5
4
4.5

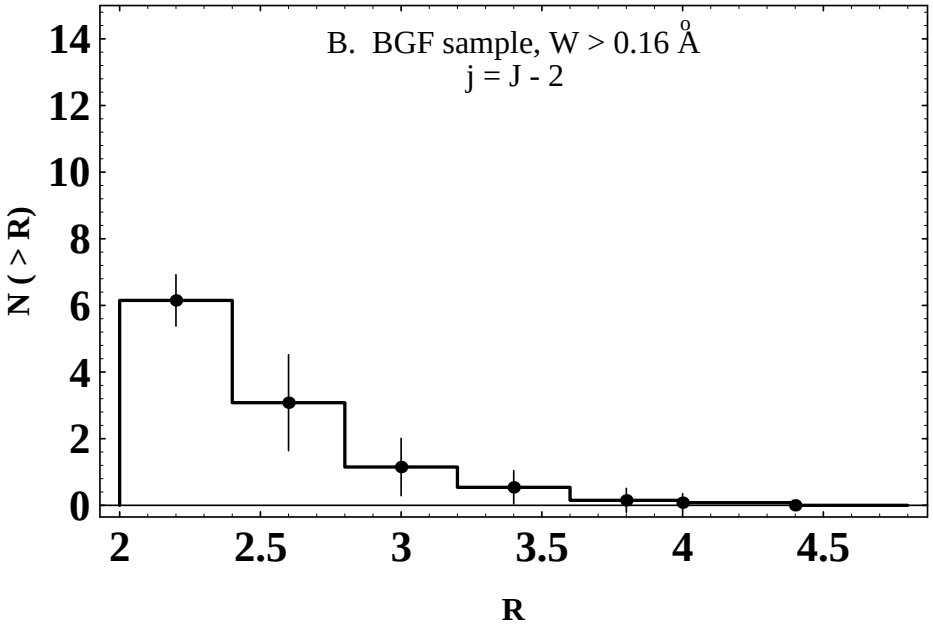
B. BGF sample, W > 0.16 Å
j = J - 2
N ( > R)
R
0
2
4
6
8
10
12
14
2
2.5
3
3.5
4
4.5

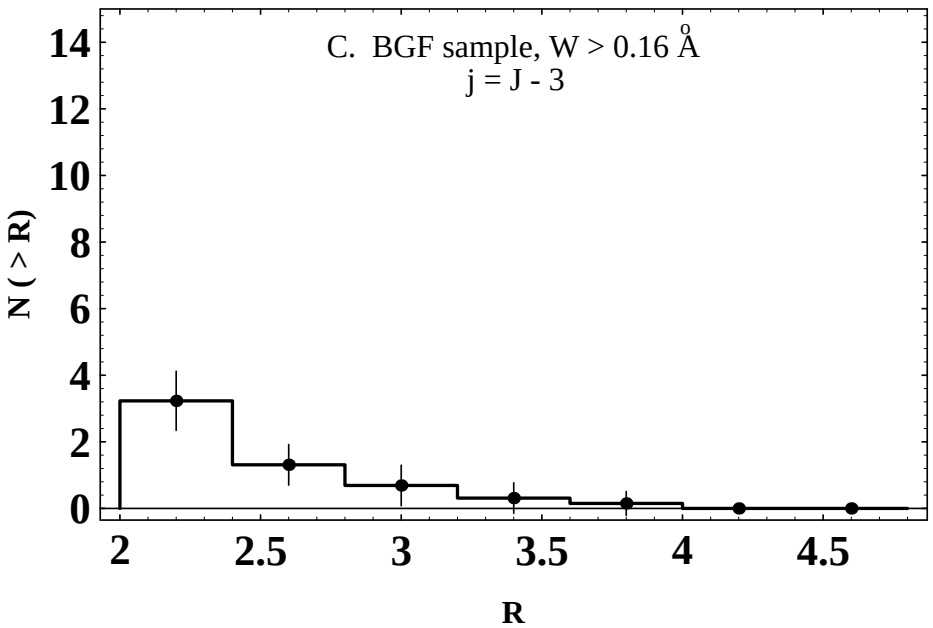
C. BGF sample, W > 0.16 Å
j = J - 3
N ( > R)
R
0
2
4
6
8
10
12
14
2
2.5
3
3.5
4
4.5

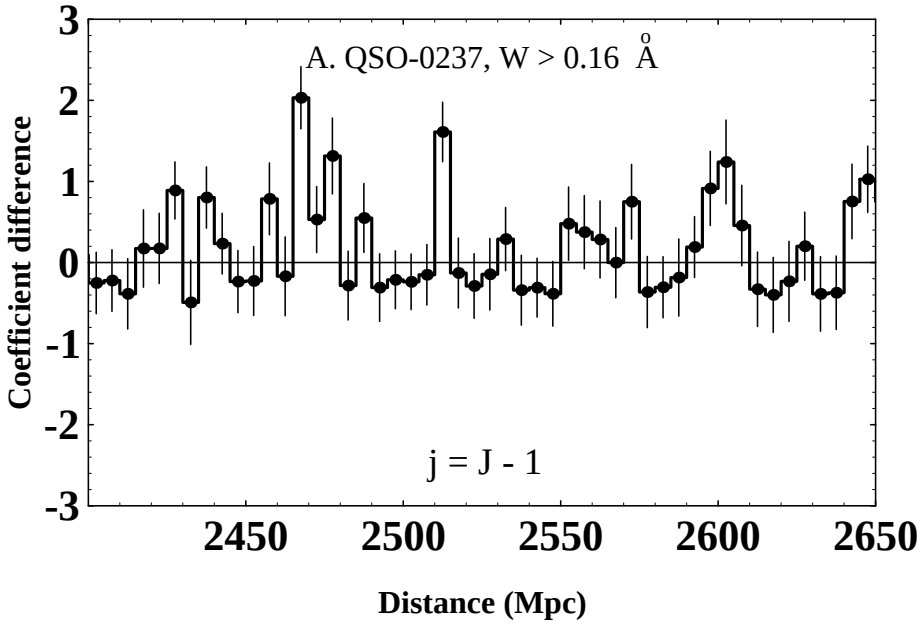
A. QSO-0237, W > 0.16 Å
Coefficient difference
3
2
1
0
-1
-2
-3
j = J - 1
2450
2500
2550
2600
2650
Distance (Mpc)

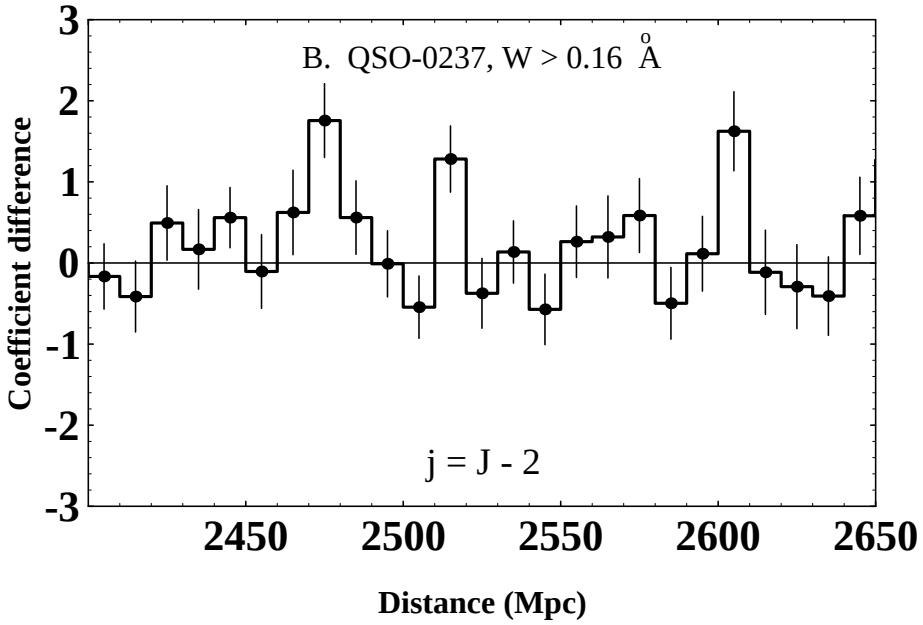
B. QSO-0237, W > 0.16 Å
Coefficient difference
3
2
1
0
-1
-2
-3
j = J - 2
2450
2500
2550
2600
2650
Distance (Mpc)

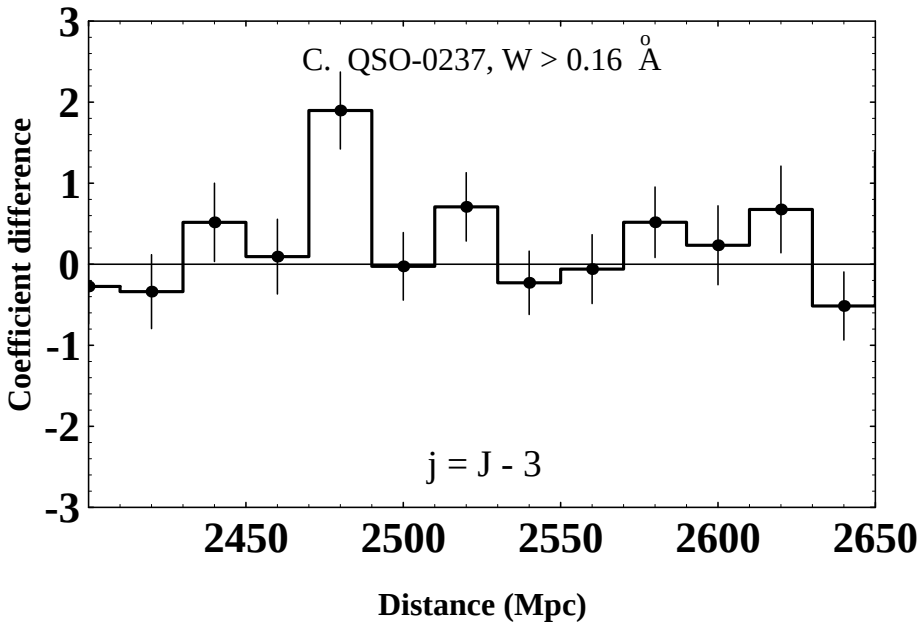
C. QSO-0237, W > 0.16 Å
Coefficient difference
3
2
1
0
-1
-2
-3
j = J - 3
2450
2500
2550
2600
2650
Distance (Mpc)

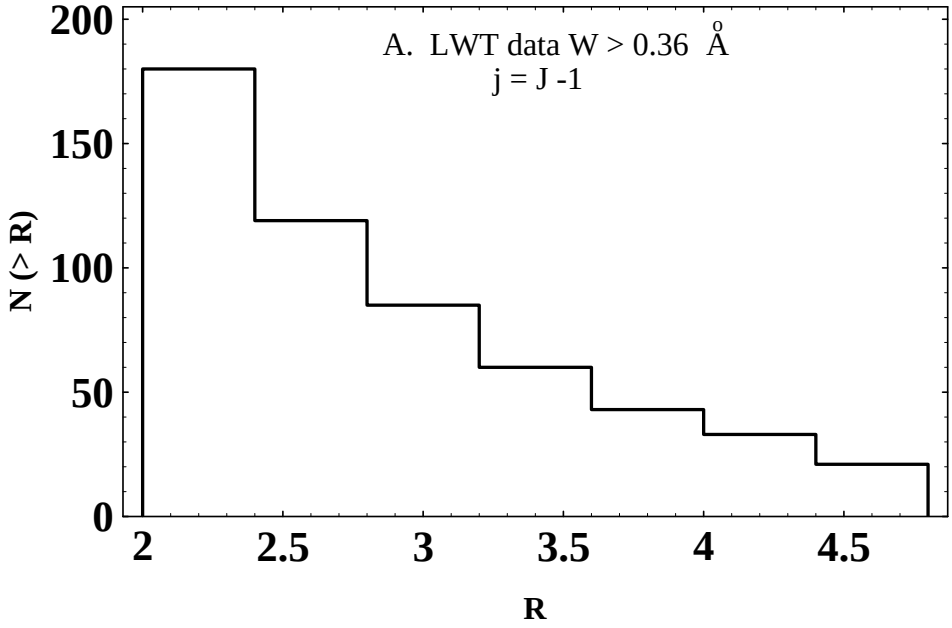
A. LWT data W > 0.36 Å
j = J -1
N (> R)
R
200
150
100
50
0
2
2.5
3
3.5
4
4.5

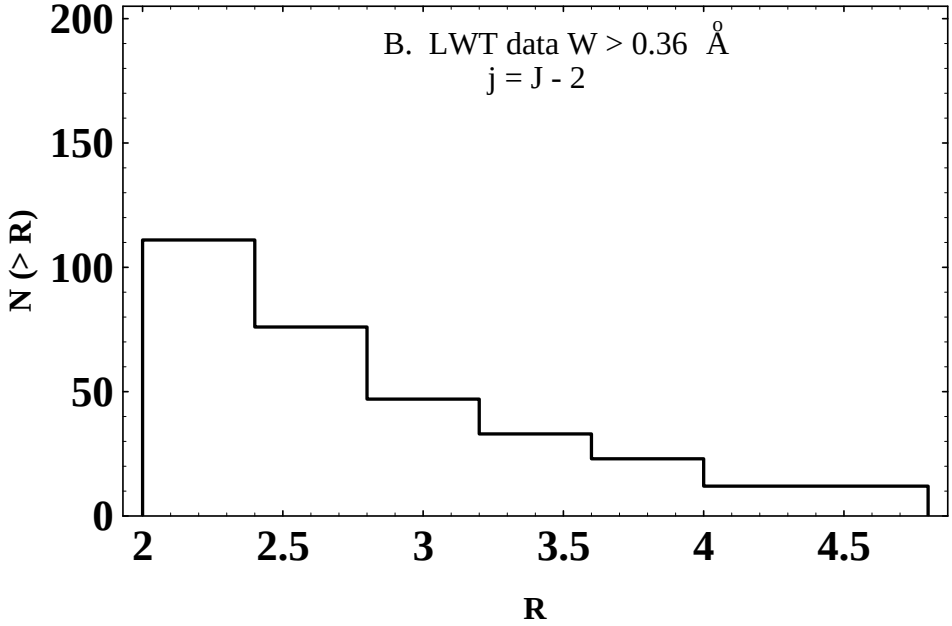
B. LWT data W > 0.36 Å
j = J - 2
N (> R)
R
200
150
100
50
0
2
2.5
3
3.5
4
4.5

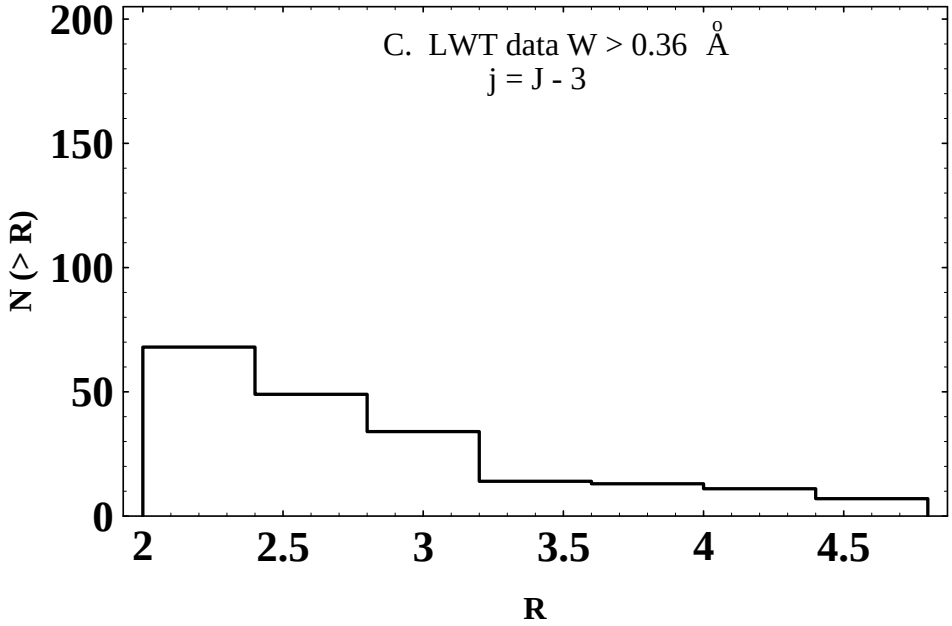
C. LWT data W > 0.36 Å
j = J - 3
N (> R)
R
200
150
100
50
0
2
2.5
3
3.5
4
4.5

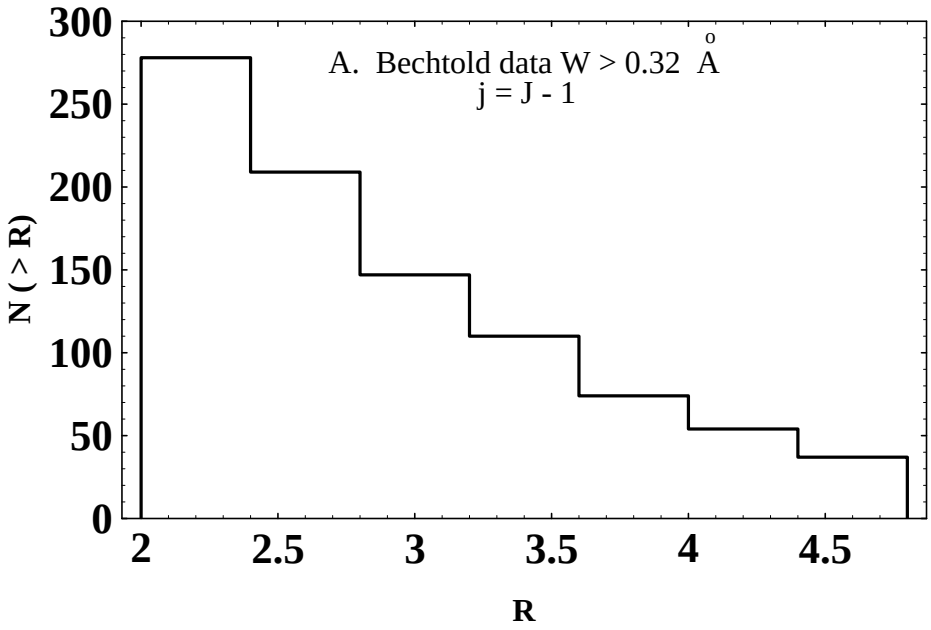
A. Bechtold data W > 0.32 Å
j = J - 1
N ( > R)
R
300
250
200
150
100
50
0
2
2.5
3
3.5
4
4.5

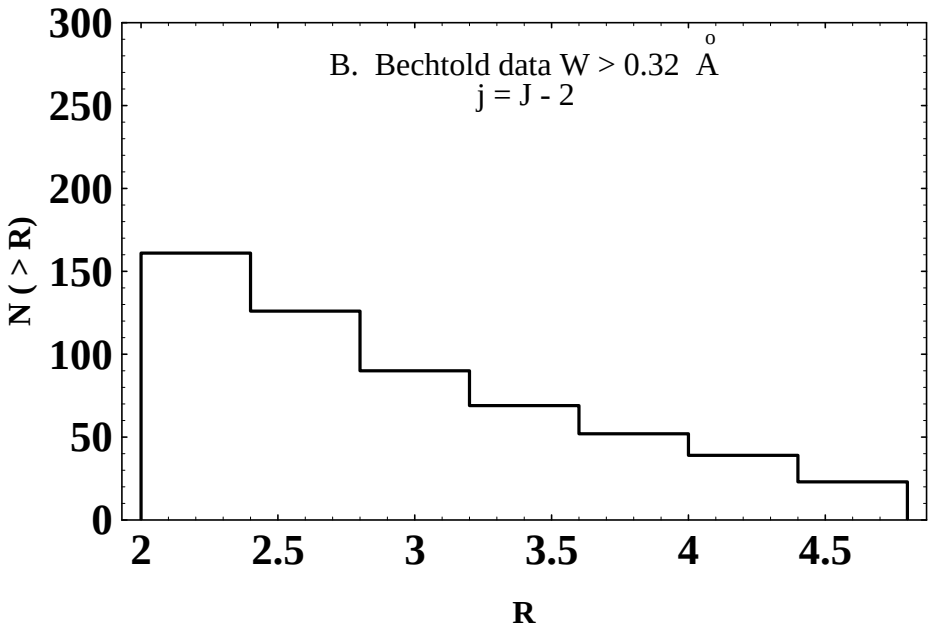
B. Bechtold data W > 0.32 Å
j = J - 2
N ( > R)
R
300
250
200
150
100
50
0
2
2.5
3
3.5
4
4.5

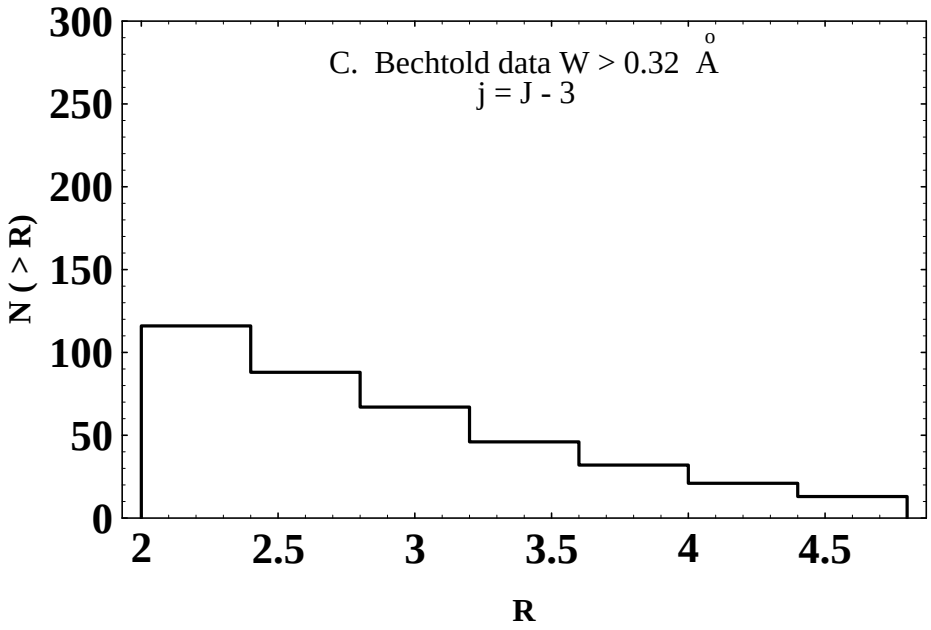
C. Bechtold data W > 0.32 Å
j = J - 3
N ( > R)
R
300
250
200
150
100
50
0
2
2.5
3
3.5
4
4.5

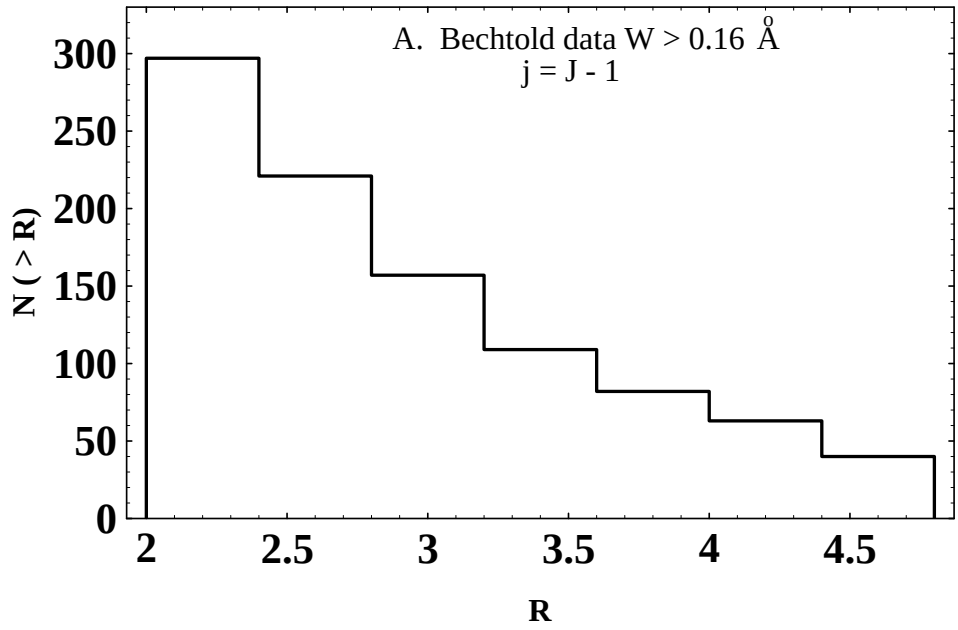
A. Bechtold data W > 0.16 Å
j = J - 1
N ( > R)
300
250
200
150
100
50
0
2
2.5
3
3.5
4
4.5
R

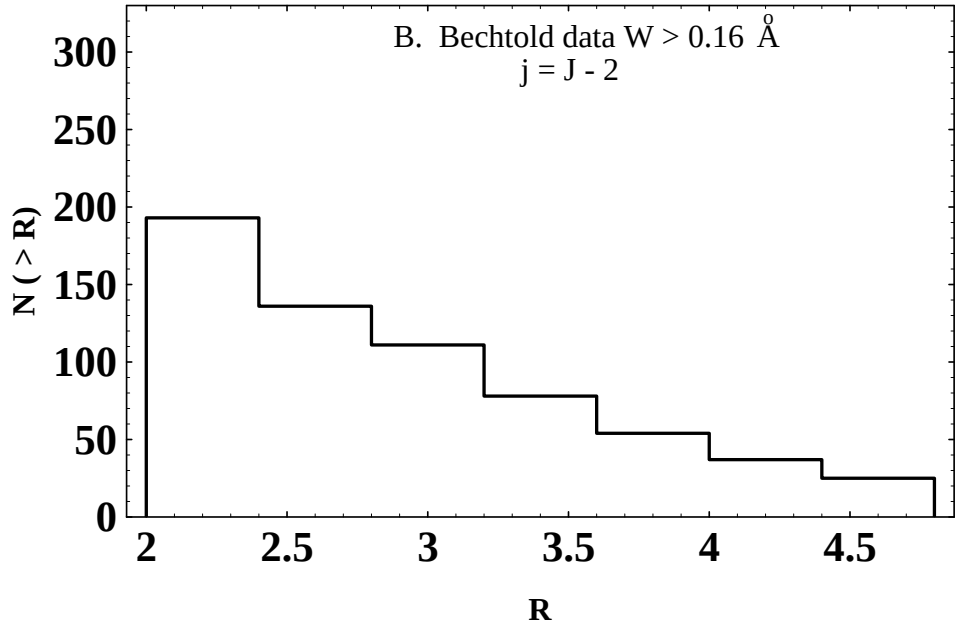
B. Bechtold data W > 0.16 Å
j = J - 2
N ( > R)
300
250
200
150
100
50
0
2
2.5
3
3.5
4
4.5
R

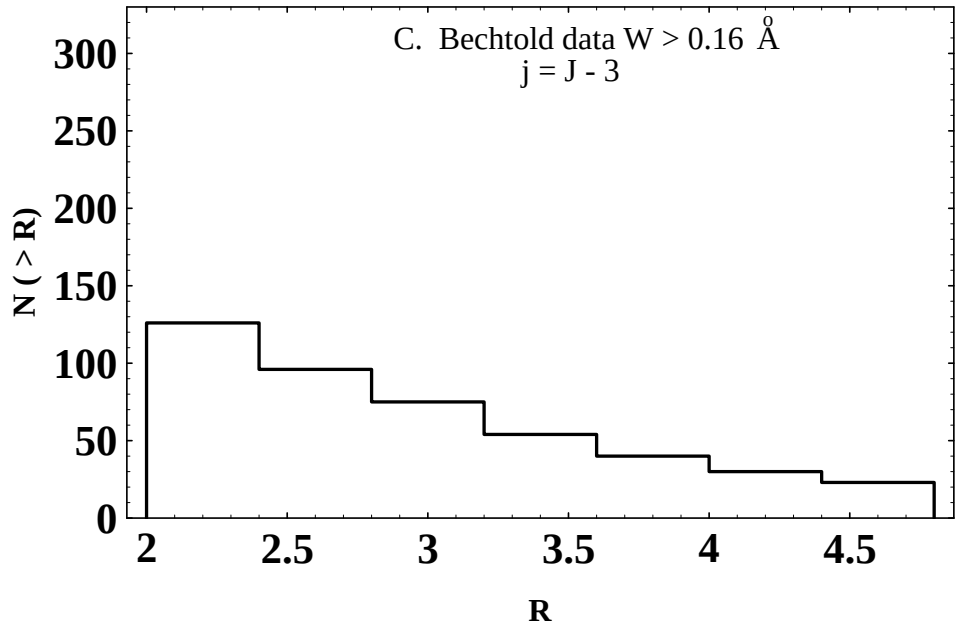
C. Bechtold data W > 0.16 Å
j = J - 3
N ( > R)
300
250
200
150
100
50
0
2
2.5
3
3.5
4
4.5
R

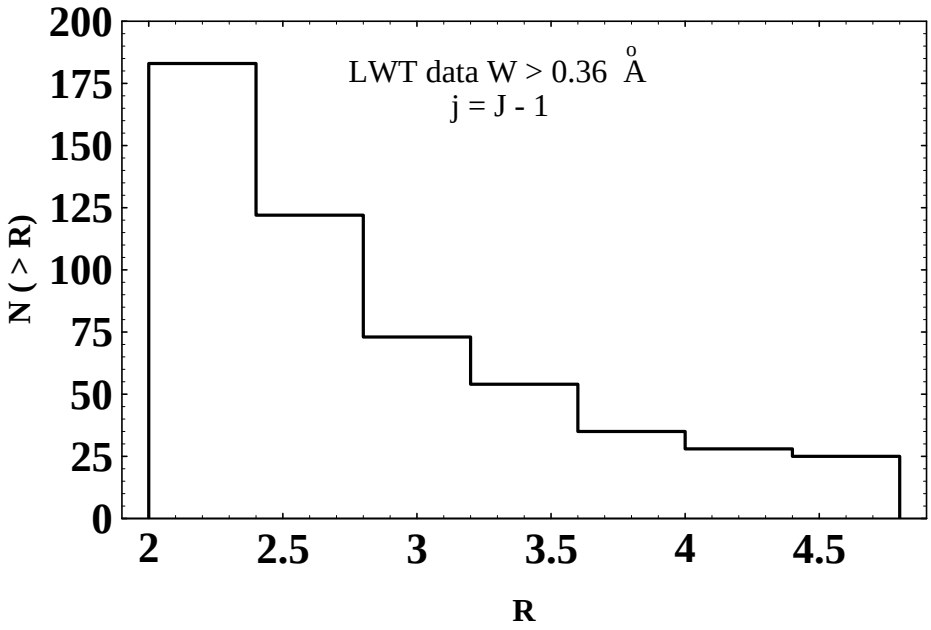
LWT data W > 0.36 Å
j = J - 1
N ( > R)
R
200
175
150
125
100
75
50
25
0
2
2.5
3
3.5
4
4.5

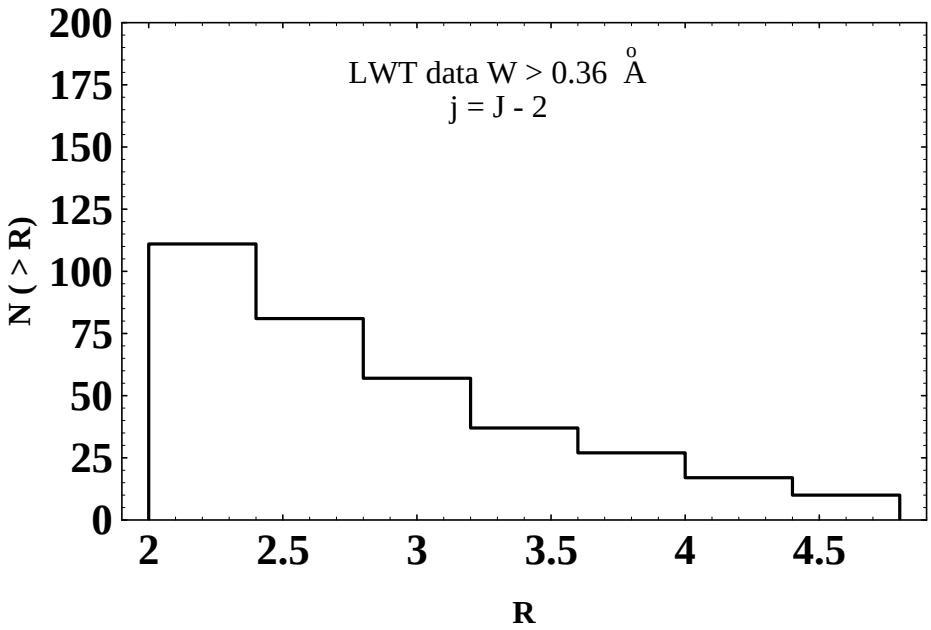
LWT data W > 0.36 Å
j = J - 2
N ( > R)
R
200
175
150
125
100
75
50
25
0
2
2.5
3
3.5
4
4.5

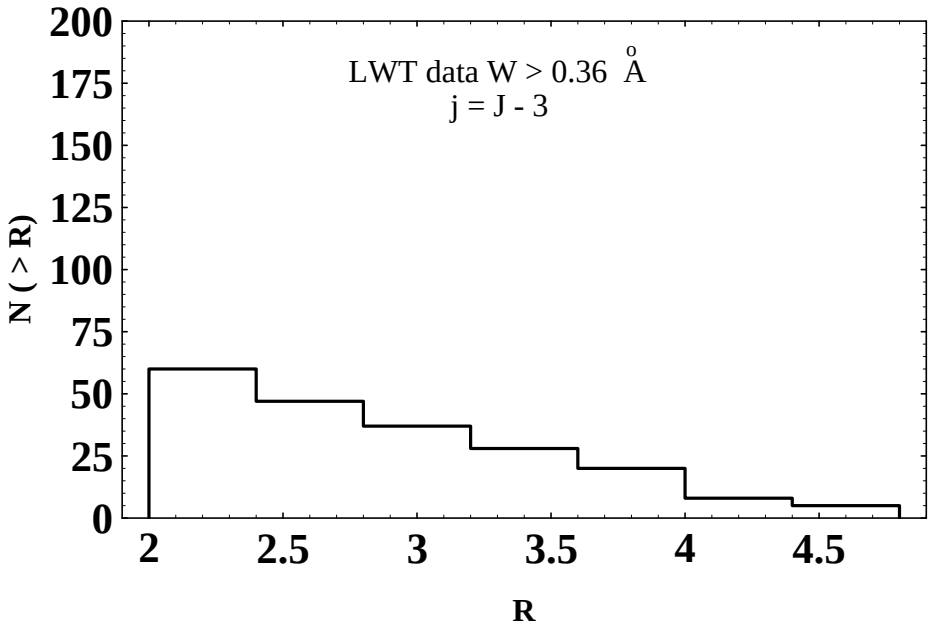
LWT data W > 0.36 Å
j = J - 3
N ( > R)
R
200
175
150
125
100
75
50
25
0
2
2.5
3
3.5
4
4.5

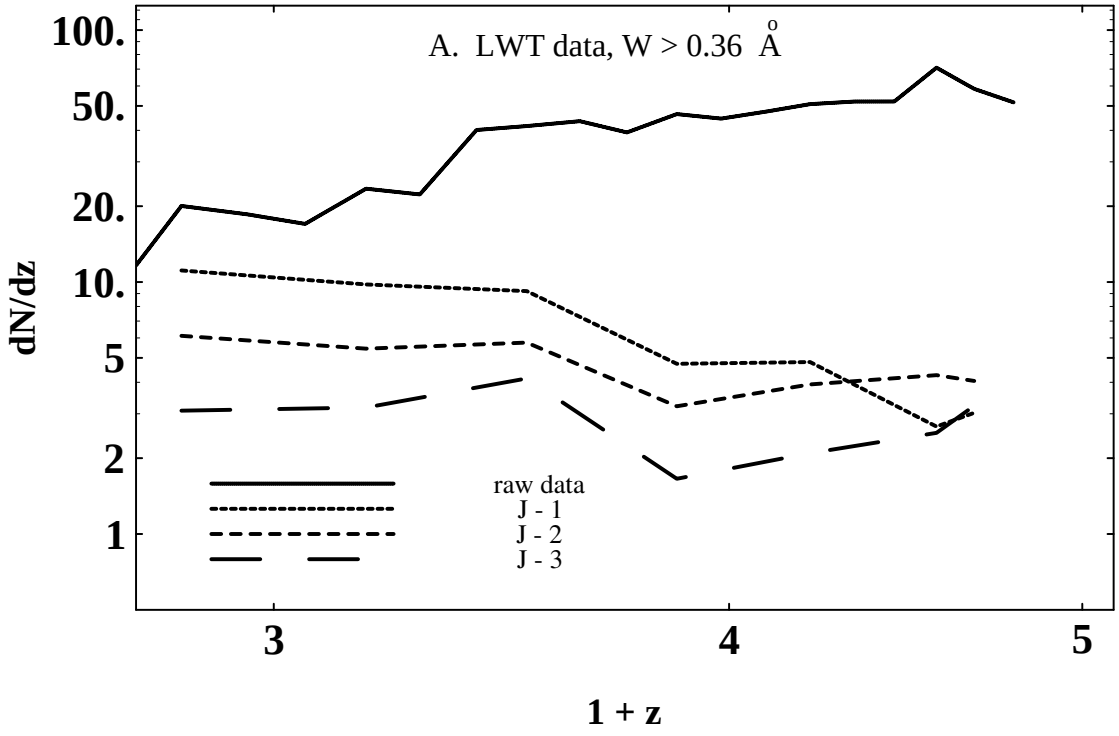
A. LWT data, W > 0.36 Å
100.
50.
20.
10.
5
2
1
dN/dz
raw data
J - 1
J - 2
J - 3
3
4
5
1 + z

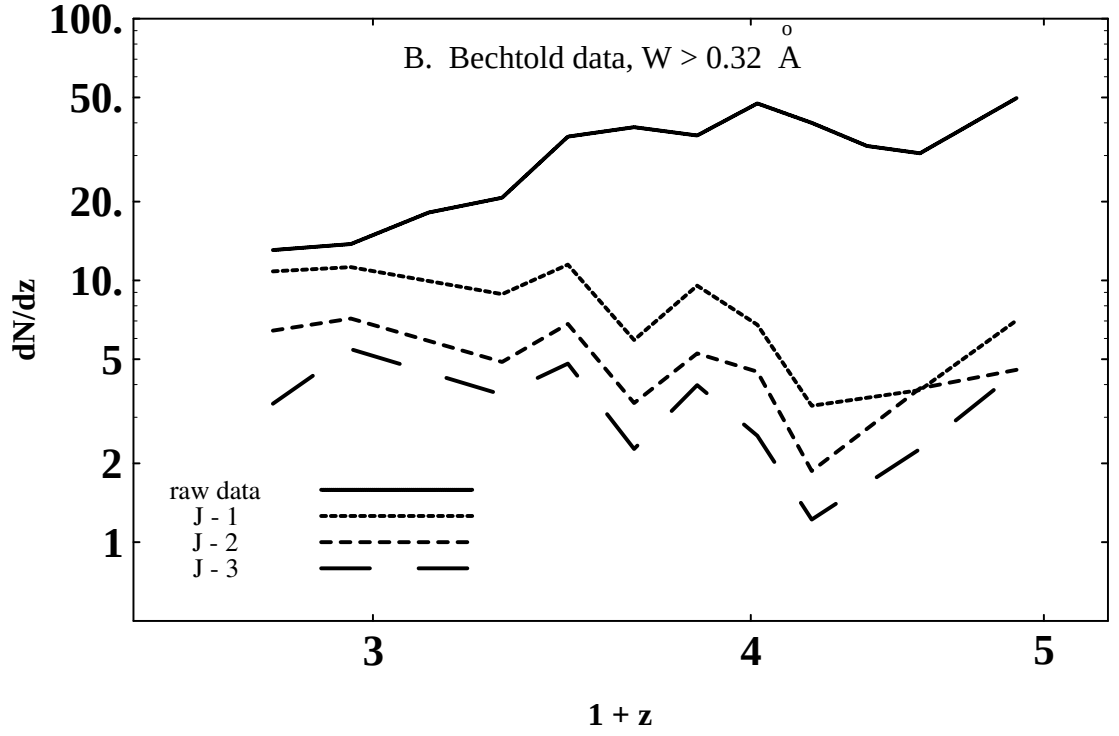
B. Bechtold data, W > 0.32 Å
100.
50.
20.
10.
5
2
1
dN/dz
raw data
J - 1
J - 2
J - 3
3
4
5
1 + z

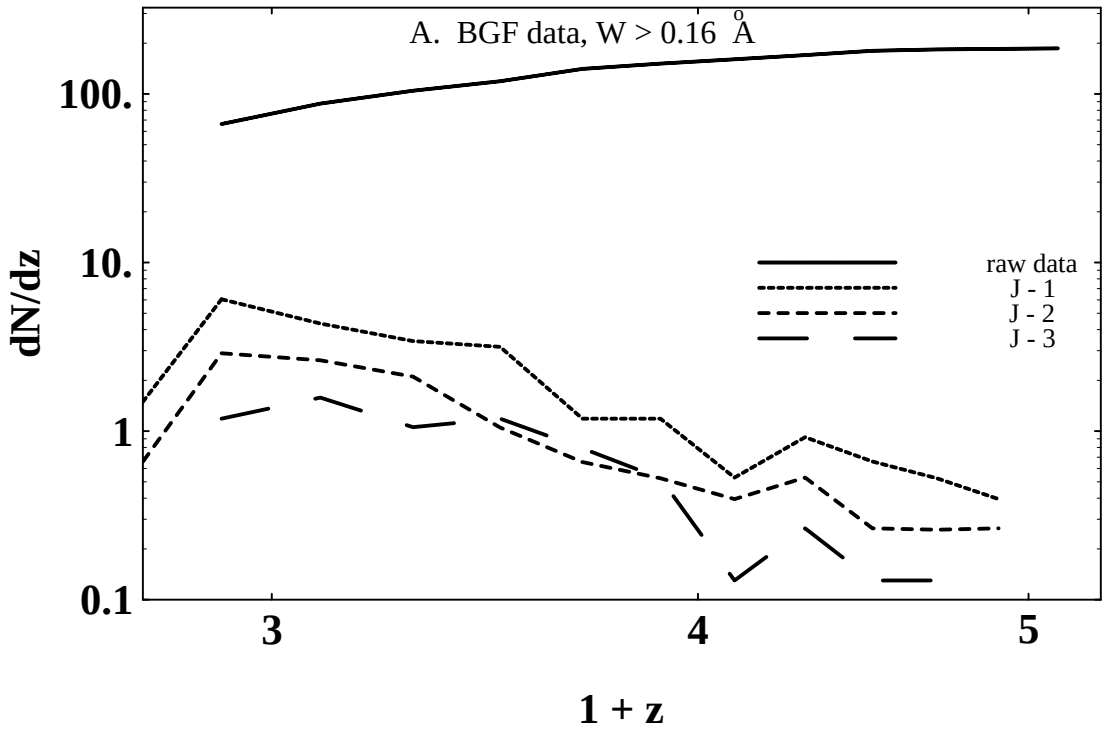
A. BGF data, W > 0.16 Å
100.
10.
1
0.1
dN/dz
raw data
J - 1
J - 2
J - 3
3
4
5
1 + z

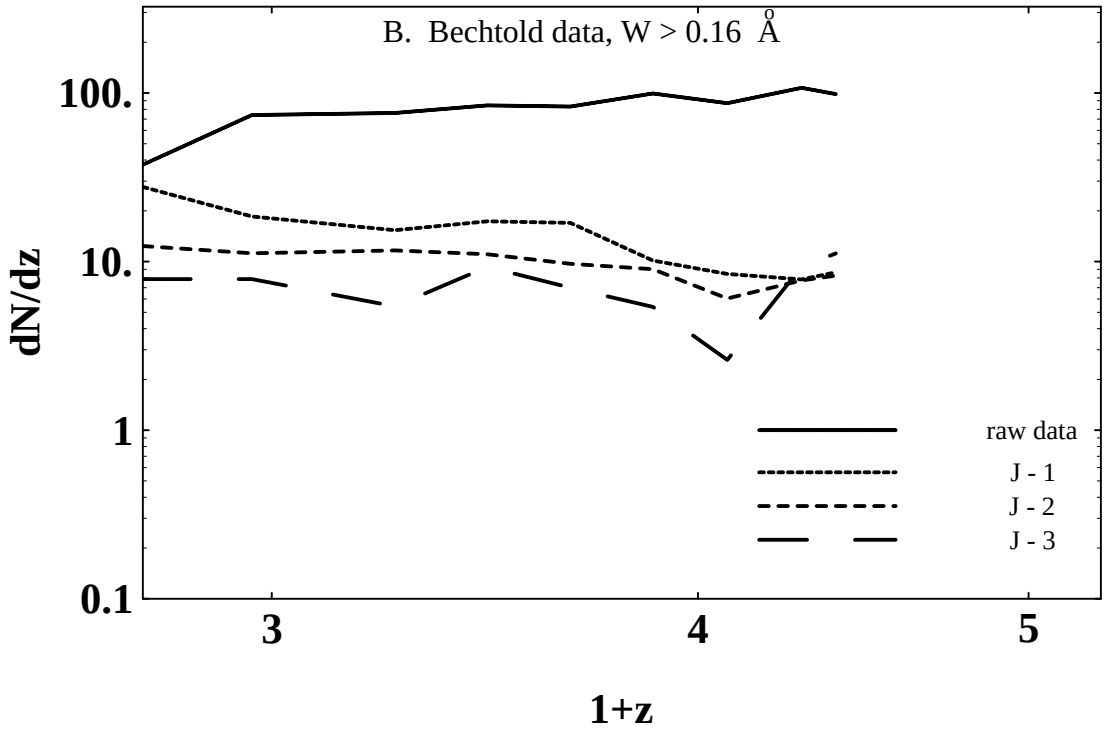
B. Bechtold data, W > 0.16 Å
100.
10.
1
0.1
dN/dz
raw data
J - 1
J - 2
J - 3
3
4
5
1+z